ATLAS CONF Note

CONF-SUSY-2017-039

2nd June 2017

Search for electroweak production of supersymmetric particles in the two and three lepton final state at $\sqrt{s} = 13$ TeV with the ATLAS detector

The ATLAS Collaboration

A search for the electroweak production of charginos, neutralinos and sleptons decaying to final states involving two or three electrons or muons is presented. The analysis is based on 36.1 fb^{-1} of $\sqrt{s}$=13 TeV proton-proton collisions recorded by the ATLAS detector at the Large Hadron Collider. No significant deviations from the Standard Model expectation are observed and results are interpreted in a range of scenarios based on simplified models. Considered scenarios include the associated production of mass-degenerate next-to-lightest neutralino and lightest chargino, followed by their decays to final-state leptons and lightest neutralinos via either sleptons or Standard Model gauge bosons; direct production of chargino pairs, which in turn decay to leptons and lightest neutralinos via intermediate sleptons; and slepton pair production, where each slepton decays directly to the lightest neutralino and a lepton. Stringent limits at 95% confidence level are placed on the masses of relevant supersymmetric particles in each of these scenarios.

1 Introduction

Supersymmetry (SUSY) [1–7] is one of the most studied extensions of the Standard Model (SM). In its minimal realisation (the Minimal Supersymmetric Standard Model, or MSSM) [8, 9], it predicts a new bosonic (fermionic) partner for each fundamental SM fermion (boson), as well as an additional Higgs doublet. These new SUSY particles, or sparticles, can provide an elegant solution to the gauge hierarchy problem [10–13]. In R-parity conserving models [14], sparticles can only be produced in pairs and the lightest supersymmetric particle (LSP) is stable. This is typically the lightest neutralino[1] $\tilde{\chi}_1^0$, which can then provide a natural candidate for dark matter [15, 16]. When produced in the decay of heavier SUSY particles, a neutralino LSP would escape detection, leading to an amount of missing transverse momentum (of magnitude E_T^{miss}) significantly larger than for SM processes, a characteristic that can be exploited to extract SUSY signals.

The production cross-sections of SUSY particles at the Large Hadron Collider (LHC) [17] depends both on the type of interaction involved and on the masses of the sparticles. The coloured sparticles (squarks and gluinos) are produced in strong interactions with significantly larger production cross-sections than non-coloured sparticles of equal masses, such as the charginos and neutralinos and the sleptons ($\tilde{\ell}$ and $\tilde{\nu}$). The direct production of charginos and neutralinos or sleptons pairs can dominate SUSY production at the LHC if the masses of the gluinos and the squarks are significantly larger. With searches performed by the ATLAS [18] and CMS [19] experiments during LHC Run II, the exclusion limits on coloured sparticle masses extend up to approximately 2 TeV [20, 21], making electroweak production an increasingly promising probe for SUSY signals at the LHC.

This paper presents a set of searches for the electroweak production of charginos, neutralinos and sleptons decaying to final states with two or three leptons (here taken to be electrons or muons only, including electrons and muons from tau decay where relevant), using 36.1 fb^{-1} of proton-proton collision data delivered by the LHC at a centre-of-mass energy of $\sqrt{s}$=13 TeV. The results build on studies performed during LHC Run I by the ATLAS collaboration [22–24]. Analogous studies by the CMS collaboration are presented in Refs. [25, 26].

After descriptions of the considered SUSY scenarios (Section 2), the experimental apparatus (Section 3), the simulated samples (Section 4) and the object reconstruction (Section 5), details of the analysis are given in Section 6. This is followed by Section 7, which describes the estimation of SM contributions to the measured yields in the signal regions, and by Section 8, which discusses systematic uncertainties affecting the current searches. Results are presented in Section 9, together with the statistical tests used to interpret them in the context of relevant SUSY benchmark scenarios. Section 10 summarises the main conclusions.

2 SUSY scenarios

This paper uses simplified models [27] to explore the direct production of $\tilde{\chi}_1^+ \tilde{\chi}_1^-$, $\tilde{\chi}_1^\pm \tilde{\chi}_2^0$ and $\tilde{\ell}\tilde{\ell}$ pairs, in instances where heavier sparticles decay to final states including exactly two or three leptons (electrons or muons), two lightest neutralinos and possibly additional SM objects (jets or neutrinos). In simplified

---

[1] The SUSY partners of the Higgs boson(known as higgsinos) and the electroweak gauge bosons (the bino for the U(1) gauge boson and winos for the W bosons) mix to form the mass eigenstates known as charginos ($\tilde{\chi}_l^\pm$, $l = 1, 2$, ordered by increasing mass) and neutralinos ($\tilde{\chi}_m^0$, $m = 1, \ldots, 4$, also ordered by increasing mass)

models, the masses of the relevant sparticles are the only free parameters. In this paper, the pure wino $\tilde{\chi}_1^\pm$ and $\tilde{\chi}_2^0$ are taken to be mass-degenerate, and so are the scalar partners of the left-handed charged leptons and neutrinos. Intermediate slepton masses, when relevant, are chosen to be midway between the mass of the heavier charginos and neutralinos and that of the $\tilde{\chi}_1^0$, which is pure bino. For models exploring $\tilde{\chi}_1^+ \tilde{\chi}_1^-$ production, it is assumed that the sleptons are also light and thus accessible in the sparticle decay chains, as illustrated in Figure 1(a). Two different classes of models are considered for $\tilde{\chi}_1^\pm \tilde{\chi}_2^0$ production: in one case, $\tilde{\chi}_1^\pm$ and $\tilde{\chi}_2^0$ can decay to final-state SM particles plus $\tilde{\chi}_1^0$ via an intermediate left-handed charged slepton or a sneutrino, with a branching ratio of 50% each (Figure 1(b)); in the other case the $\tilde{\chi}_1^\pm$ and $\tilde{\chi}_2^0$ decay happens via SM gauge bosons (W/Z) (Figures 1(d)-1(e)). In models with direct $\tilde{\ell}\tilde{\ell}$ production, each slepton decays to lepton-$\tilde{\chi}_1^0$ with a 100% branching ratio (Figure 1(c)), and left-handed and right-handed selectrons, smuons and staus are assumed to be degenerate. For the gauge-boson-mediated decays two distinct final states are considered: three-lepton events where both the W and Z boson decay leptonically; or events with two opposite-sign leptons and two jets where the W boson decays hadronically and the Z boson decays leptonically. Tree-level diagrams of considered processes are shown in Figure 1.
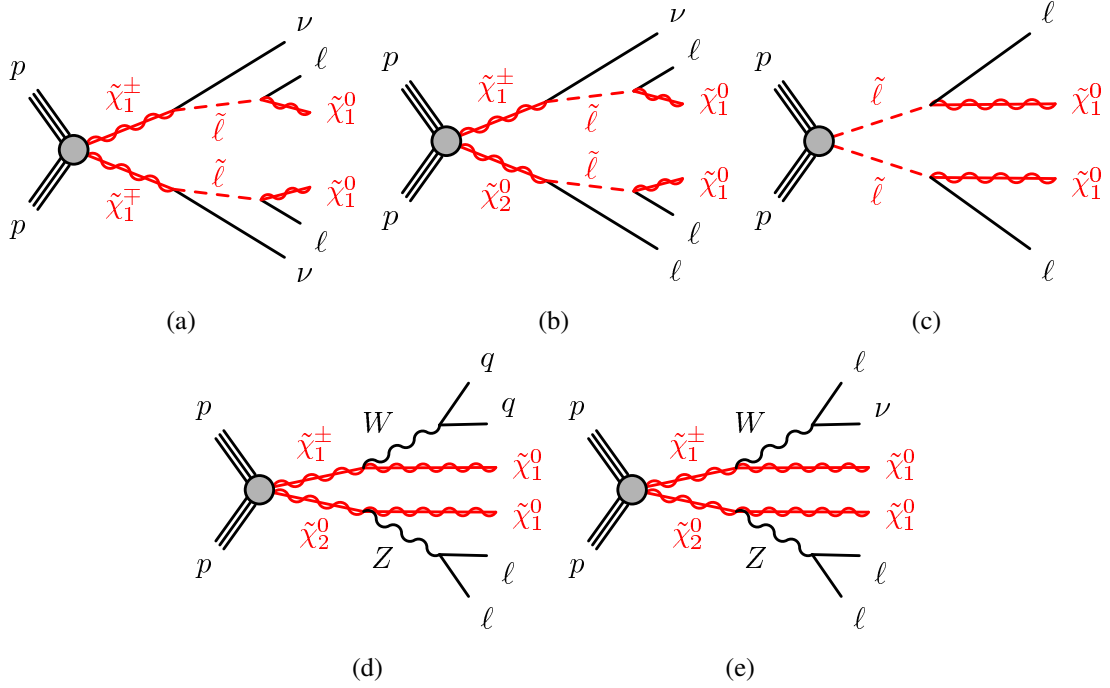

Figure 1: Diagrams of the physics scenarios studied in this paper: (a) $\tilde{\chi}_1^+ \tilde{\chi}_1^-$ with $\tilde{\ell}$-mediated decays, (b) $\tilde{\chi}_1^\pm \tilde{\chi}_2^0$ with $\tilde{\ell}$-mediated decays, (c) direct-slepton pair production, (d) $\tilde{\chi}_1^\pm \tilde{\chi}_2^0$ with decays via a hadronically decaying W boson and a leptonically decaying Z boson to final states with two leptons and two jets and (e) $\tilde{\chi}_1^\pm \tilde{\chi}_2^0$ with decays via leptonically decaying W and Z bosons to final states with three leptons.

3 ATLAS detector

The ATLAS experiment [18] is a multi-purpose particle detector with a forward-backward symmetric cylindrical geometry and nearly 4π coverage in solid angle.[2] The interaction point is surrounded by an inner detector (ID), a calorimeter system, and a muon spectrometer.

The ID provides precision tracking of charged particles for pseudorapidities $|\eta| < 2.5$ and is surrounded by a superconducting solenoid providing a 2 T axial magnetic field. It consists of pixel and silicon-microstrip detectors inside a transition radiation tracker. One significant upgrade for the $\sqrt{s} = 13$ TeV running period is the installation of the Insertable B-Layer [28], an additional pixel layer close to the interaction point, which provides high-resolution hits at small radius to improve the tracking performance.

In the pseudorapidity region $|\eta| < 3.2$, high-granularity lead/liquid-argon (LAr) electromagnetic (EM) sampling calorimeters are used. A steel/scintillator tile calorimeter measures hadron energies for $|\eta| < 1.7$. The endcap and forward regions, spanning $1.5 < |\eta| < 4.9$, are instrumented with LAr calorimeters, for both the EM and hadronic measurements.

The muon spectrometer consists of three large superconducting toroids with eight coils each, and a system of trigger and precision-tracking chambers, which provide triggering and tracking capabilities in the ranges $|\eta| < 2.4$ and $|\eta| < 2.7$, respectively.

A two-level trigger system is used to select events [29]. The first-level trigger is implemented in hardware and uses a subset of the detector information. This is followed by the software-based High-Level Trigger stage, which can run offline reconstruction and calibration software, reducing the event rate to about 1 kHz.

4 Data and simulated samples

This analysis uses data delivered by the LHC at $\sqrt{s} = 13$ TeV in 2015 and 2016. After fulfilling data-quality requirements, the data sample amounts to an integrated luminosity of 36.1 fb^{-1} with an uncertainty of $\pm 3.2\%$ derived using a methodology similar to that detailed in Refs. [30, 31], from a preliminary calibration of the luminosity scale using x-y beam-separation scans performed in August 2015 and May 2016.

Various samples of Monte Carlo (MC) simulated events are used to model the SUSY signal and help in the estimation of the SM backgrounds. The samples include an ATLAS detector simulation [32], based on Geant4 [33], or a fast simulation that uses a parametrisation of the calorimeter response and Geant4 for the other parts of the detector [34]. The simulated events are reconstructed in the same manner as the data.

SM diboson processes are simulated with the Sherpa v2.2.1 generator [35, 36]. The matrix elements contain all diagrams with four electroweak vertices with additional hard parton emissions calculated with

---

[2] ATLAS uses a right-handed coordinate system with its origin at the nominal interaction point (IP) in the centre of the detector and the z-axis along the beam pipe. The x-axis points from the IP to the centre of the LHC ring, and the y-axis points upward. Cylindrical coordinates (r, ϕ) are used in the transverse plane, ϕ being the azimuthal angle around the beam pipe. The pseudorapidity is defined in terms of the polar angle θ as $\eta = -\ln\tan(\theta/2)$. Rapidity is defined as $y = 0.5\ln\left[(E + p_z)/(E - p_z)\right]$ where E denotes the energy and p_z is the component of the momentum along the beam direction.

Comix [37] and virtual QCD corrections calculated with OpenLoops [38] . Matrix element calculations are merged with the Sherpa parton shower [39] using the ME+PS@NLO prescription [40]. The NNPDF3.0nnlo PDF [41] set is used in conjunction with dedicated parton shower tuning developed by the Sherpa authors. The fully-leptonic channels are calculated at next-to-leading order (NLO) in the strong coupling constant with up to one additional parton for 4ℓ and $2\ell + 2\nu$, at NLO with no additional parton for $3\ell + \nu$, and at leading order (LO) with up to three additional partons. Processes with one of the bosons decaying hadronically and the other leptonically are calculated with up to one additional parton at NLO and up to three additional partons at LO.

Diboson processes with six electroweak vertices, such as same-electric-charge W boson production in association with two jets, $W^{\pm}W^{\pm}jj$, and triboson processes are simulated with Sherpa v2.1.1, the CT10 PDF set [42], and similar use of Comix, OpenLoops, Sherpa parton shower, and ME+PS@NLO as the Sherpa v2.2.1 samples described above. Six vertex diboson processes are calculated at LO with up to one additional parton. Fully leptonic triboson processes (WWW, WWZ, WZZ and ZZZ) are calculated at LO with up to two additional partons and at NLO for the inclusive processes.

Events containing Z bosons and associated jets (Z/γ^*+jets, also referred to as Z+jets in the following) are produced using the Sherpa v2.2.1 generator with massive b/c-quarks to improve the treatment of the associated production of Z bosons with jets containing b- and c-hadrons [43]. Matrix elements are calculated with up to two additional partons at NLO and up to four additional partons at LO. The matrix elements are calculated using the Comix and OpenLoops generators and merged with the Sherpa parton shower using the ME+PS@NLO prescription. A global k-factor is used to normalise the Z+jets events to the next-to-next-to-leading order (NNLO) QCD cross-sections [44].

For the production of $t\bar{t}$ and single top-quarks in the Wt channel, the Powheg-Box v2 [45, 46] generator with the CT10 PDF set [42] is used [47]. The top quark mass is assumed to be 172.5 GeV. The $t\bar{t}$ events are normalised to the NNLO+next-to-next-to-leading logarithm (NNLL) QCD [48] cross-sections, while the cross-section for single-top events is calculated at NLO+NNLL [49].

Samples of $t\bar{t}V$ (with $V = W$ and Z, including non-resonant Z/γ^* contributions) and $t\bar{t}WW$ production are generated at LO with MadGraph v2.2.2 [50] interfaced to the Pythia 8.186 [51] parton shower model, with up to two ($t\bar{t}W$), one ($t\bar{t}Z$) or no ($t\bar{t}WW$) extra partons included in the matrix element, as described in detail in Ref. [52]. MadGraph is also used to simulate the tZ, $t\bar{t}t\bar{t}$ and $t\bar{t}t$ processes. The A14 set of tuned parameters from [53] is used together with the NNPDF23LO PDF set [54]. The $t\bar{t}W$, $t\bar{t}Z$, $t\bar{t}WW$ and $t\bar{t}t\bar{t}$ events are normalised to their NLO cross-section [50] while the generator cross-section is used for tZ and $t\bar{t}t$.

Higgs boson production processes (including gluon-gluon fusion, associated production VH and vector boson fusion, VBF) are generated using Powheg v2 [55] + Pythia 8.186, whilst $t\bar{t}H$ events are produced using aMC@NLO 2.3.2 + Pythia 8.186. All samples assume a Higgs mass of 125 GeV.

The SUSY signal processes are generated from LO matrix elements with up to two extra partons, using the MadGraph v2.2.3 generator interfaced to Pythia 8.186 with the A14 tune for the modelling of the SUSY decay chain, parton showering, hadronisation and the description of the underlying event. Parton luminosities are provided by the NNPDF23LO PDF set. Jet–parton matching is realised following the CKKW-L prescription [56], with a matching scale set to one quarter of the pair-produced superpartner mass. Signal cross-sections are calculated at NLO in the strong coupling constant, with soft gluon emission effects added at next-to-leading-logarithmic (NLL) accuracy [57–61]. The nominal cross-section and the uncertainty are taken from an envelope of cross-section predictions using different PDF sets and factorisation and renormalisation scales, as described in Ref. [62]. The production cross-section

of $\tilde{\chi}_1^+ \tilde{\chi}_1^-$ each with a mass of 600 GeV is 9.50 fb at $\sqrt{s} = 13$ TeV (compared with 1.96 fb at $\sqrt{s} = 8$ TeV), while the production cross-section of pairs of $\tilde{\chi}_1^\pm \tilde{\chi}_2^0$ each with a mass of 800 GeV is 4.76 fb at $\sqrt{s} = 13$ TeV (compared with 0.68 fb at $\sqrt{s} = 8$ TeV).

In all MC samples, except those produced by SHERPA, the EvtGen v1.2.0 program [63] is used to model the properties of the bottom and charm hadron decays. To simulate the effects of additional pp collisions in the same and nearby bunch crossings (pileup), additional interactions are generated using the soft QCD processes of PYTHIA 8.186 with the A2 tune [64] and the MSTW2008LO PDF set [65], and overlaid onto the simulated hard scatter event. The Monte Carlo samples are reweighted so that the distribution of the number of reconstructed vertices matches the distribution observed in data.

5 Event reconstruction and pre-selection

Events used in the analysis are recorded during stable data-taking conditions and must have a reconstructed primary vertex [66] with at least two associated tracks with $p_T > 400$ MeV. The primary vertex of an event is identified as the vertex with the highest Σp_T^2 of associated tracks.

Two identification criteria are defined for the objects used in these analyses, referred to as "baseline" and "signal" (with the "signal" objects being a subset of the baseline ones). The former are defined in order to perform data-driven non-prompt leptonic background estimates (discussed in Section 7) while the latter are used when defining regions where SUSY signals are enhanced.

Baseline electrons are reconstructed from isolated electromagnetic calorimeter energy deposits matched to ID tracks and are required to have $|\eta| < 2.47$, a transverse momentum $p_T > 10$ GeV, and to pass a loose likelihood-based identification requirement [67, 68]. The likelihood input variables include measurements of calorimeter shower shapes and track properties from the ID.

Baseline muons are reconstructed in the region $|\eta| < 2.5$ from muon spectrometer tracks matching ID tracks. All muons must have $p_T > 10$ GeV and must pass the medium identification requirements defined in Ref. [69], based on selections on the number of hits in the different ID and muon spectrometer subsystems, and the significance of the charge to momentum ratio q/p [69].

Jets are reconstructed with the anti-k_t algorithm [70] with radius parameter $R = 0.4$, using three-dimensional energy clusters in the calorimeter [71] as input. All jets must have $p_T > 20$ GeV and $|\eta| < 2.8$. Jets are calibrated as described in Ref. [72]. In order to reduce the effects of pileup, jets with $p_T < 60$ GeV and $|\eta| < 2.4$ must have a significant fraction of their associated tracks compatible with originating from the primary vertex, as defined by the jet vertex tagger [73]. Furthermore, for all jets the expected average energy contribution from pileup clusters is subtracted according to the jet area [72].

Identification (b-tagging) of jets containing b-hadrons (b-jets) is performed with the MV2c10 algorithm, a multivariate discriminant making use of track impact parameters and reconstructed secondary vertices [74, 75]. A requirement is chosen corresponding to a 77% average efficiency obtained for b-jets in simulated $t\bar{t}$ events.

Photon candidates are required to pass the "tight" selection criteria of [76] and satisfy $p_T > 25$ GeV and $|\eta| < 2.37$, but excluding the region $1.37 < |\eta| < 1.52$ (this is the "transition region" where there is a discontinuity in the calorimeter).

After object identification, an "object-removal procedure" is performed on all baseline objects to remove possible double-counting in the reconstruction:

1. Any electron sharing an ID track with a muon is removed.
2. If a b-tagged jet is within $\Delta R = \sqrt{(\Delta y)^2 + (\Delta \phi)^2} = 0.2$ of an electron candidate, the electron is rejected, as it is likely to be from a semileptonic b-decay; if the jet within $\Delta R = 0.2$ of the electron is not b-tagged, the jet itself is discarded, as it likely originates from an electron-induced shower.
3. Electrons within $\Delta R = 0.4$ of a jet candidate are discarded, to suppress electrons from semileptonic decays of c- and b-hadrons.
4. Jets with fewer than three associated tracks are discarded
5. Jets with a nearby muon that carries a significant fraction of the transverse momentum of the jet ($p_T^\mu > 0.7 \sum p_T^{\text{jet tracks}}$, where p_T^μ and $p_T^{\text{jet tracks}}$ are the transverse momenta of the muon and tracks associated with the jet, respectively) are discarded either if the candidate muon is within $\Delta R = 0.2$ or if the muon is matched to a track associated with the jet.
6. Muons within $\Delta R = 0.4$ of a jet candidate are discarded to suppress muons from semileptonic decays of c- and b-hadrons.

Signal electrons must satisfy a medium likelihood-based identification requirement [67] and the track associated with the electron must have a significance of the transverse impact parameter with respect to the reconstructed primary vertex, d_0, of $|d_0|/\sigma(d_0) < 5$, with $\sigma(d_0)$ being the uncertainty on d_0. In addition, the longitudinal impact parameter (again with respect to the reconstructed primary vertex), z_0, must satisfy $|z_0 \sin\theta| < 0.5$ mm. Similarly, signal muons must satisfy the requirements of $|d_0|/\sigma(d_0) < 3$ and $|z_0 \sin\theta| < 0.5$ mm. Isolation requirements are also applied to both the signal electrons and muons to reduce the contributions of "fake" or non-prompt leptons, which originate from misidentified hadrons, photon conversions, and decays-in-flight and semi-leptonic decays of hadrons. These p_T-dependent requirements use track-based and calorimeter information and have efficiencies in $Z \rightarrow e^+ e^-$ and $Z \rightarrow \mu^+ \mu^-$ events that rise from 95% at 25 GeV to 99% at 60 GeV.

Signal photons are required to have $p_T > 37$ GeV and must also satisfy p_T-dependent requirements on both track- and calorimeter-based isolation.

The missing transverse energy E_T^{miss} is defined as the magnitude of the two-dimensional vector, $\boldsymbol{p}_T^{\text{miss}}$, which is the negative vector sum of the transverse momenta of all identified physics objects (electrons, photons, muons, jets) and an additional soft term. The soft term is constructed from all tracks that are not associated with any physics object, and which are associated with the primary vertex. The E_T^{miss} is adjusted for the best calibration of the jets and the other identified physics objects above, while maintaining pileup independence in the soft term [77, 78].

Events considered in the analysis must pass a trigger selection requiring either two electrons, two muons or an electron plus a muon. Such events must be triggered by one of the lowest unprescaled di-leptonic triggers. The trigger-level requirements on the p_T of the leptons involved in the trigger decision (the p_T thresholds range between 8-22 GeV) are looser than those applied offline to ensure that trigger efficiencies are constant in the relevant phase space. Events are discarded if they contain any jet failing basic quality selection criteria that reject detector noise and non-collision backgrounds. Simulated events are corrected to account for minor differences in the signal lepton trigger, reconstruction, identification and isolation efficiencies between data and MC simulation, as well as for differences in b-tagging efficiency between data and MC.

6 Search strategy

In order to search for the electroweak production of supersymmetric particles three different search channels are defined which relate to the three different signatures:

- **2ℓ+0jets:** targets $\tilde{\chi}_1^+ \tilde{\chi}_1^-$ and $\tilde{\ell}\tilde{\ell}$ pair production (shown in Figures 1(a) and 1(c)) in signal regions with a jet veto and defined using the "stransverse mass" variable, m_{T2} [79, 80], and the di-lepton invariant mass $m_{\ell\ell}$;

- **2ℓ+jets:** targets $\tilde{\chi}_1^\pm \tilde{\chi}_2^0$ pair production with decays via gauge bosons (shown in Figure 1(d)) to two same-flavour opposite-sign (SFOS) leptons (from the Z boson) and at least 2 jets (from the W boson);

- **3ℓ:** targets $\tilde{\chi}_1^\pm \tilde{\chi}_2^0$ pair production with decays via intermediate $\tilde{\ell}$ or gauge bosons to three lepton final states (shown in Figures 1(b) and 1(e)).

In each channel, the signal regions (SRs) require exactly two or three signal leptons (as defined in the previous section), with vetos on any additional baseline leptons. The leading and sub-leading leptons are required to have $p_{\text{T}} > 25$ GeV and 20 GeV respectively; however, in the 2ℓ+jets and 3ℓ channels additional (tighter) lepton p_{T} requirements are applied.

In the 2ℓ+0jets channel the leptons are required to be of opposite sign and events are separated into "same flavour" (SF) events (corresponding to di-electron, e^+e^-, and di-muon, $\mu^+\mu^-$, events) and "different flavour" (DF) events (electron-muon, $e^\pm\mu^\mp$). This division is driven by the different background-compositions of the two classes of events. All events are required to have a di-lepton invariant mass $m_{\ell\ell} > 40$ GeV and a veto is applied on the following orthogonal jet categories:

- Central non-b-tagged jets: $p_{\text{T}} > 60$ GeV, $|\eta| < 2.4$ and not b-tagged.

- Central b-tagged jets: $p_{\text{T}} > 20$ GeV, $|\eta| < 2.4$ and b-tagged.

These jet categories are also used when defining control regions to determine the normalisation of the diboson and $t\bar{t}$ backgrounds as described in Section 7. After this pre-selection, binned signal regions are used to maximise exclusion sensitivity across the $\tilde{\chi}_1^+ \tilde{\chi}_1^-$ pair production and direct-$\tilde{\ell}$ pair production grids. In the SF regions a two-dimensional binning in m_{T2} and $m_{\ell\ell}$ is used as this provides strong rejection against the Z/γ+jets background, whereas in the DF regions, where the Z/γ+jets background is negligible, a one-dimensional binning in m_{T2} is sufficient. The stransverse mass m_{T2} is defined as:

$$m_{\text{T2}} = \min_{\mathbf{q}_{\text{T}}} \left[\max \left(m_{\text{T}}(\mathbf{p}_{\text{T}}^{\ell 1}, \mathbf{q}_{\text{T}}), m_{\text{T}}(\mathbf{p}_{\text{T}}^{\ell 2}, \mathbf{p}_{\text{T}}^{\text{miss}} - \mathbf{q}_{\text{T}}) \right) \right],$$

where $\mathbf{p}_{\text{T}}^{\ell 1}$ and $\mathbf{p}_{\text{T}}^{\ell 2}$ are the transverse momentum vectors of the two leptons, and $\mathbf{q}_{\text{T}}$ is a transverse vector that minimizes the larger of $m_{\text{T}}(\mathbf{p}_{\text{T}}^{\ell 1}, \mathbf{q}_{\text{T}})$ and $m_{\text{T}}(\mathbf{p}_{\text{T}}^{\ell 2}, \mathbf{p}_{\text{T}}^{\text{miss}} - \mathbf{q}_{\text{T}})$, where:

$$m_{\text{T}}(\mathbf{p}_{\text{T}}, \mathbf{q}_{\text{T}}) = \sqrt{2(p_{\text{T}} q_{\text{T}} - \mathbf{p}_{\text{T}} \cdot \mathbf{q}_{\text{T}})}.$$

The m_{T2} variable provides good suppression of SM $t\bar{t}$ and WW backgrounds, which have expected kinematic endpoints at the W-boson mass. The definitions of the binned signal regions are provided in Table 1. When producing model-dependent exclusion limits in the $\tilde{\chi}_1^+ \tilde{\chi}_1^-$ simplified model grid, all signal regions are statistically combined, whereas only the same flavour regions are used when probing direct-$\tilde{\ell}$

production. In addition, a set of inclusive signal regions are also defined, which are used to provide a more model-independent test for an excess of events. The definitions of these regions are also provided in Table 1.

2ℓ+0jets binned signal region definitions			
m_{T2}[GeV]	$m_{\ell\ell}$ [GeV]	SF bin	DF bin
100-150	111-150	SR2-SF-a	SR2-DF-a
	150-200	SR2-SF-b	
	200-300	SR2-SF-c	
	> 300	SR2-SF-d	
150-200	111-150	SR2-SF-e	SR2-DF-b
	150-200	SR2-SF-f	
	200-300	SR2-SF-g	
	> 300	SR2-SF-h	
200-300	111-150	SR2-SF-i	SR2-DF-c
	150-200	SR2-SF-j	
	200-300	SR2-SF-k	
	> 300	SR2-SF-l	
> 300	> 111	SR2-SF-m	SR2-DF-d
2ℓ+0jets inclusive signal region definitions			
> 100	> 111	SR2-SF-loose	-
> 130	> 300	SR2-SF-tight	-
> 100	-	-	SR2-DF-100
> 150	-	-	SR2-DF-150
> 200	-	-	SR2-DF-200
> 300	-	-	SR2-DF-300

Table 1: The definitions of the binned and inclusive signal regions for the 2ℓ+0jets channel.

In the 2ℓ+jets channel two inclusive signal regions, denoted SR2-int and SR2-high, are used to target intermediate and large mass splittings between the $\tilde{\chi}_1^\pm/\tilde{\chi}_2^0$ and the LSP. In addition to the pre-selection used in the 2ℓ+0jets channel (minus the non-b-tagged jet veto requirement), the sub-leading lepton is also required to have $p_{\mathrm{T}} > 25$ GeV and events must have at least two signal jets with $p_{\mathrm{T}} > 30$ GeV. A b-jet veto is also applied (defined in the same way as in the 2ℓ+0jets channel). Many of the selection requirements defining these regions are used to select two leptons consistent with an on-shell Z boson and two jets consistent with a W boson. A tight requirement on m_{T2} is also used to suppress the $t\bar{t}$ background. After these selection requirements, the SM backgrounds are suppressed by other requirements on $E_{\mathrm{T}}^{\mathrm{miss}}$ which provide sensitivity to the SUSY processes of interest. An additional region, denoted SR2-low, is also defined to target lower mass splittings (in particular, the region of parameter space around {m($\tilde{\chi}_1^\pm$)=m($\tilde{\chi}_2^0$), m($\tilde{\chi}_1^0$)} = {200,100} GeV). It is split into two orthogonal sub-regions which are merged when presenting the results in Section 9. SR2-low-2J requires exactly two jets which are both assumed to originate from the W boson, while the SR2-low-3J requires 3–5 signal jets and assumes the $\tilde{\chi}_1^\pm \tilde{\chi}_2^0$ system recoils against initial-state-radiation (ISR) jets. The two jets originating from the W boson are selected to be those closest to the $Z (\to \ell\ell) + E_{\mathrm{T}}^{\mathrm{miss}}$ system that have a mass m_{jj} consistent with the mass of the W boson. This is different to SR2-int and SR2-high, where the two jets leading in p_{T} in the event are used to define the W boson candidate. All regions use angular variables to select the signal topologies of interest, in the case

of SR2-low: a W boson recoiling against the $Z+E_\mathrm{T}^\mathrm{miss}$ system for SR2-low-2J and a $W+Z+E_\mathrm{T}^\mathrm{miss}$ system recoiling against ISR jets in SR2-low-3J. The definitions of the signal regions in the 2ℓ+jets channel are summarised in Table 2.

2ℓ+jets signal region definitions				
	SR2-int	SR2-high	SR2-low-2J	SR2-low-3J
$n_{\mathrm{non}-b-\mathrm{tagged\ jets}}$	≥ 2		2	3-5
$m_{\ell\ell}$ [GeV]	81-101		81-101	86-96
m_{jj} [GeV]	70-100		70-90	70-90
$E_\mathrm{T}^\mathrm{miss}$ [GeV]	>150	> 250	>100	>100
p_T^Z [GeV]	>80		> 60	> 40
p_T^W [GeV]	>100			
m_T2 [GeV]	>100			
$\Delta R_{(jj)}$	<1.5			<2.2
$\Delta R_{(\ell\ell)}$	<1.8			
$\Delta\phi_{(\vec{E}_\mathrm{T}^\mathrm{miss},Z)}$			< 0.8	
$\Delta\phi_{(\vec{E}_\mathrm{T}^\mathrm{miss},W)}$	0.5-3.0		> 1.5	< 2.2
$E_\mathrm{T}^\mathrm{miss}/p_\mathrm{T}^Z$			0.6 − 1.6	
$E_\mathrm{T}^\mathrm{miss}/p_\mathrm{T}^W$			< 0.8	
$\Delta\phi_{(\vec{E}_\mathrm{T}^\mathrm{miss},\mathrm{ISR})}$				> 2.4
$\Delta\phi_{(\vec{E}_\mathrm{T}^\mathrm{miss},\mathrm{jet1})}$				> 2.6
$E_\mathrm{T}^\mathrm{miss}/\mathrm{ISR}$				0.4-0.8
$|\eta(Z)|$				< 1.6
$p_\mathrm{T}^\mathrm{jet3}$ [GeV]				> 30

Table 2: Signal region definitions used for the 2ℓ+jets channel. The abbreviations W and Z correspond to the reconstructed W- and Z-bosons in the final state. The Z-boson is always reconstructed from the two leptons, whereas the W-boson is reconstructed from the two jets leading in p_T for SR2-int, SR2-high and the 2-jets channel of SR2-low, whilst for the 3-5 jets channel of SR2-low it is reconstructed from the two jets which combine to be closest in a $\Delta R(= \sqrt{\Delta\eta^2 + \Delta\phi^2})$ cone to the $Z (\to \ell\ell) + E_\mathrm{T}^\mathrm{miss}$ system. ISR refers to the vectorial sum of the initial-state-radiation jets in the event (i.e. those not used in the W reconstruction) and jet1 and jet3 refer to the leading and third leading jet respectively.

The 3ℓ channel targets $\tilde{\chi}_1^\pm \tilde{\chi}_2^0$ pair production and uses kinematic variables such as $E_\mathrm{T}^\mathrm{miss}$ and the transverse mass m_T, which were used in the Run-I analysis [23]. Events are required to have exactly three baseline leptons satisfying the signal lepton requirements and zero b-tagged jets. In addition, two of the leptons must form a SFOS pair (as expected in $\tilde{\chi}_2^0 \to \ell^+\ell^- \tilde{\chi}_1^0$ decays). To resolve ambiguities when multiple SFOS pairings are present, the transverse mass value of the unpaired lepton is calculated for each possible SFOS pairing and the lepton that yields the minimum transverse mass is assigned to the W boson. This transverse mass value is denoted by $m_\mathrm{T}^\mathrm{min}$, and is used alongside $E_\mathrm{T}^\mathrm{miss}$, jet multiplicity (in the gauge-boson-mediated scenario) and other relevant kinematic variables to define binned signal regions that have sensitivity to $\tilde{\ell}$-mediated and gauge-boson-mediated decays. The definitions of these binned regions are provided in Table 3. The bins denoted "slep-a,b,c,d,e" target $\tilde{\ell}$-mediated decays and consequently have a veto on SFOS pairs with an invariant mass consistent with the Z boson (this suppresses the WZ background). The invariant mass of the SFOS pair, $m_{\ell\ell}$, the missing transverse momentum, $E_\mathrm{T}^\mathrm{miss}$, and the p_T of the third leading lepton, $p_\mathrm{T}^{\ell_3}$, are used to define the SR bins. Conversely, the bins denoted "WZ-0Ja,b,c" and "WZ-1Ja,b,c" target gauge-boson mediated-decays and thus require the SFOS pair to have an invariant

mass consistent with an on-shell Z boson. The 0-jet and $\geq$ 1-jet channels are considered separately and the regions are binned in $m_\mathrm{T}^\mathrm{min}$ and $E_\mathrm{T}^\mathrm{miss}$.

			3ℓ binned signal region definitions				
m_SFOS [GeV]	$E_\mathrm{T}^\mathrm{miss}$ [GeV]	$p_\mathrm{T}^{\ell_3}$ [GeV]	$n_{\mathrm{non}-b-\mathrm{tagged\ jets}}$	$m_\mathrm{T}^\mathrm{min}$ [GeV]	$p_\mathrm{T}^{\ell\ell}$ [GeV]	$p_\mathrm{T}^\mathrm{jet1}$ [GeV]	Bins
<81.2	> 130	20-30 > 30		> 110			SR3-slep-a SR3-slep-b
>101.2	> 130	20-50 50-80 > 80		> 110			SR3-slep-c SR3-slep-d SR3-slep-e
81.2-101.2	60-120 120-170 > 170		0	> 110			SR3-WZ-0Ja SR3-WZ-0Jb SR3-WZ-0Jc
81.2-101.2	120-200 > 200	> 35	$\geq$ 1	> 110 110-160 > 160	< 120	> 70	SR3-WZ-1Ja SR3-WZ-1Jb SR3-WZ-1Jc

Table 3: Summary of the binned signal regions used in the 3ℓ channel. The bins labelled "slep" target slepton-mediated decays whereas those labelled "WZ" target gauge-boson-mediated decays. $p_\mathrm{T}^{\ell_3}$ refers to the p_T of the third leading lepton and $p_\mathrm{T}^\mathrm{jet1}$ denotes the p_T of the leading signal jet.

7 Background estimation and validation

The SM backgrounds contributing in the two- and three-lepton final states can be classified into irreducible backgrounds which contain processes leading to events with prompt and isolated leptons, and reducible backgrounds, which contain events that either contain at least one "fake" or non-prompt (denoted FNP) lepton, or where experimental effects (e.g., detector mismeasurement of objects, usually jets) lead to significant "fake" $E_\mathrm{T}^\mathrm{miss}$. An FNP lepton is a non-prompt lepton that can originate from a semi-leptonic decay of a b- or c-hadron, from misidentification of a light-flavoured jet, or from a photon conversion. A summary of the background estimation techniques used in each channel is provided in Table 4. In the 2ℓ+0jets and 3ℓ final states the dominant backgrounds are normalized in dedicated control regions (CRs) which are included, together with the SRs, in simultaneous likelihood fits to data to extract the final results. In the 2ℓ+jets channel no CRs are used, and the likelihood fits include the SRs only. The likelihood fits are described in more detail in Section 9.

For the two-lepton channels the dominant backgrounds are irreducible processes including SM diboson production (WW,WZ and ZZ), Z/γ+jets and $t\bar{t}$, where diboson processes dominate the 2ℓ+0jets channel whereas the 2ℓ+jets channel is dominated by SM processes that give an on-shell Z boson (i.e. diboson and Z/γ+jets). For the 2ℓ+0jets channel MC is used to predict kinematic distributions for these backgrounds, but the $t\bar{t}$ and diboson backgrounds are then normalised to data in dedicated control regions. For the diboson backgrounds SF and DF events are treated separately and two control regions are defined. The first one (CR2-VV-SF) selects SFOS lepton pairs with an invariant mass consistent with the Z boson mass and has a hard requirement on $m_\mathrm{T2} > 130$ GeV to reduce the Z/γ+jets contamination. This region is dominated by ZZ events, with subdominant contributions from WZ and WW events. The DF diboson

Background estimation summary			
Channel	2ℓ+0jets	2ℓ+jets	3ℓ
Fake leptons	Matrix method (MM)		Fake factor method (FF)
$t\bar{t} + Wt$	CR	MC	FF
VV	CR	MC	CR (WZ-only)
Z/γ+jets	MC	γ+jet template	FF
Higgs/ VVV/ top+V	MC		

Table 4: Summary of the estimation methods used in each search channel. Backgrounds denoted CR have a dedicated control region that is included in a simultaneous likelihood fit to data to extract a data-driven normalisation factor that is used to scale the MC prediction. MM and FF refer to the matrix method and fake factor method used to estimate the fake lepton backgrounds in the 2ℓ and 3ℓ channels, respectively. The γ+jet template method is used in the 2ℓ+jets channel to provide a data-driven estimate of the Z/γ+jets background. Finally MC stands for pure Monte Carlo estimation.

control region (CR2-VV-DF) selects events with a DFOS pair and further requires $50 < m_{T2} < 75$ GeV. This region is dominated by WW events, with a subdominant contribution from WZ events. The $t\bar{t}$ control region (CR2-Top) uses DF events with at least one central b-tagged jet to obtain a high-purity sample of $t\bar{t}$ events. The control region definitions are summarised in Table 5.

The three control regions are included in a simultaneous profile likelihood fit to the observed data that provides data-driven normalisation factors for these backgrounds, as described in Section 9. The results are propagated to the signal regions, and to dedicated validation regions (VRs) whose selections resemble those of the signal regions while selecting a mutually exclusive set of events. The validation regions used for the 2ℓ+0jets channel are provided in Table 5. The normalisation factors returned by the fit for the $t\bar{t}$, VV-DF and VV-SF backgrounds are 0.95 ± 0.03, 1.06 ± 0.18 and 0.96 ± 0.11, respectively. In the 2ℓ+0jets channel the Z/γ+jets and Higgs boson contributions are expected to be small, and are estimated directly from MC.

2ℓ+0jets control and validation region definitions					
Region	CR2-VV-DF	CR2-VV-SF	CR2-Top	VR2-VV-SF/DF	VR2-Top
lepton flavour	SF	DF	DF	SF (DF)	DF
$n_{\text{central non}-b-\text{tagged jets}}$	0	0	0	0	0
$n_{\text{central } b-\text{tagged jets}}$	0	0	≥ 1	0	≥ 1
$\lvert m_{\ell\ell} - m_Z \rvert$ [GeV]	< 20	—	—	> 20 (–)	—
m_{T2} [GeV]	> 130	50 − 75	75 − 100	75 − 100	> 100

Table 5: Control region and validation region definitions for the 2ℓ+0jets channel. The p_T thresholds placed on the requirements for b- and non-b-tagged jets correspond to 20 GeV and 60 GeV, respectively.

In the 2ℓ+jets channel, the dominant backgrounds are Z/γ+jets and diboson events. Although expected to occur rarely, Z/γ+jets events can enter the SRs due to fake E_T^{miss} from jet or lepton mis-measurements or from neutrinos in semi-leptonic decays of b- or c- hadrons. These effects are difficult to model in MC, so instead γ+jets events in data are used to measure a E_T^{miss} template in Z+jets events. Similar methods have been employed in searches for SUSY in events with two leptons, jets, and large E_T^{miss} in ATLAS [81] and CMS [82, 83]. The E_T^{miss} shape is extracted from a data control sample of γ+jets events, which have a similar topology and E_T^{miss} resolution as Z+jets events. Corrections for the different γ vs. Z boson p_T

distributions and different momentum resolutions for electrons, muons, and photons are applied, and the shape is normalized to data in the SR-like region with $E_T^{miss} < 100$ GeV. For the $m_{\ell\ell}$ and m_{T2} quantities that depend on the individual lepton momenta, the photon is split into two pseudo-leptons, assuming isotropic decays in the boson rest frame and boosting into the detector frame.

To validate the method, as well as check the modelling of other SM backgrounds, two sets of validation regions, "tight" and "loose", are defined for each SR. The definitions of these regions (VR2-low-2J, VR2-low-3J, VR2-int, and VR2-high) are provided in Table 6. For the "tight" regions , the dijet mass m_{jj} requirement is replaced by the requirement ($m_{jj} < 60$ GeV or $m_{jj} > 100$ GeV), supressing signal, but the selections are otherwise identical to the SR selections. For VR2-int and VR2-high these "tight" regions have Z+jets background contributions that are small compared to the diboson background, hence do not effectively validate the Z+jets modelling. The second set of "loose" validation regions are therefore defined by removing several other kinematic requirements used in the SR definition (m_{T2}, all $\Delta\phi$ and ΔR quantities, and the ratios of E_T^{miss} to W p_T, Z p_T, and ISR p_T). These samples have enough Z+jets events to perform comparisons of kinematic distributions which validate the normalization and kinematic modeling of the Z+jets background.

Once the signal region requirements are applied, the dominant background in the 2ℓ+jets channel is the diboson background. This is taken from MC, but the modelling is verified in two dedicated validation regions, one for the low mass-splitting signal regions (VR2-VV-low) and one for the intermediate and high-mass signal regions (VR2-VV-int). By requiring high E_T^{miss} and exactly one signal jet (compared to at least two in the signal regions) these regions have a high diboson purity. The definitions of the diboson validation regions are provided in Table 6 along with the "loose" and "tight" validation regions defined for validating the Z/γ+jets data driven method. The remaining irreducible background components are evaluated using MC.

For both the 2ℓ+0jets and 2ℓ+jets channels, reducible background originates from FNP leptons mainly arising from multijet, W+jets and single top quark production, all of which can yield one or two FNP leptons. For both analyses, the FNP lepton background is estimated from data using the matrix method [84] (MM). This method uses two types of lepton identification criteria: "signal", corresponding to signal leptons, and "baseline" leptons, corresponding to candidate electrons and muons as defined in Section 7. The method makes use of the number of observed events containing baseline-baseline, baseline-signal, signal-baseline and signal-signal lepton pairs in a given SR. By measuring the probabilities for real and FNP leptons passing the baseline selection criteria to also pass the signal selection, the observed event counts can be used to extract data-driven estimates for the FNP lepton background for each analysis.

For the 3ℓ channel, the irreducible background is mainly dominated by SM WZ diboson processes. As in the 2ℓ+0jets channel the shape of this background is taken from MC but normalised to data in a dedicated control region. The binned signal regions shown in Table 3 include a set of binned regions inclusive in jet multiplicity that target $\tilde{\ell}$-mediated decays, and a set of regions binned in jet multiplicity targeting gauge-boson-mediated decays. To reflect this, three control regions are defined to extract the normalisation of the WZ background; an inclusive region (CR3-WZ-inc) and two binned control regions (CR3-WZ-0j and CR3-WZ-1j). When using the binned control regions, WZ events are separated into two categories: those containing zero jets and those containing at least one jet. Separate normalisation factors are then assigned to each set of events when performing the simultaneous likelihood fit, however when using the inclusive control region a single normalisation factor is obtained from the inclusive WZ control region. The normalisation factors extracted from the fit for inclusive WZ events, zero-jet WZ events and WZ events with at least one jet are 0.97 ± 0.06, 1.08 ± 0.06 and 0.94 ± 0.07, respectively. The results of the background estimates are validated in a set of dedicated validation regions. This includes

2ℓ+jets validation region definitions				
	VR2-int(high)	VR2-low-2J(3J)	VR2-VV-int	VR2-VV-low
loose selection				
$n_{\text{non}-b-\text{tagged jets}}$	≥ 2	2 (3-5)	1	1
E_T^{miss} [GeV]	>150 (250)	>100	>150	>150
$m_{\ell\ell}$ [GeV]	81-101	81-101 (86-96)		81-101
m_{jj} [GeV]	<60,>100	<60,>100		
p_T^Z [GeV]	>80	> 60(40)		
p_T^W [GeV]	>100			
$\lvert\eta(Z)\rvert$		(< 1.6)		
p_T^{jet3} [GeV]		(> 30)		
$\Delta\phi_{(\vec{E}_T^{miss},jet)}$			>0.4	>0.4
m_{T2} [GeV]	>100[*]		>100	
$\Delta R_{(\ell\ell)}$	<1.8[*]			<0.2
tight selection				
$\Delta R_{(jj)}$	<1.5	(<2.2)		
$\Delta\phi_{(\vec{E}_T^{miss},W)}$	0.5-3.0	> 1.5(< 2.2)		
$\Delta\phi_{(\vec{E}_T^{miss},Z)}$		< 0.8(−)		
E_T^{miss}/p_T^W		< 0.8(−)		
E_T^{miss}/p_T^Z		0.6 − 1.6(−)		
E_T^{miss}/ISR		(0.4 − 0.8)		
$\Delta\phi_{(\vec{E}_T^{miss},ISR)}$		(> 2.4)		
$\Delta\phi_{(\vec{E}_T^{miss},jet1)}$		(> 2.6)		

Table 6: Validation region definitions used for the 2ℓ+jets channel. The superindex, [*], refers to requirements applied in the tight selection.

two validation regions that are binned in jet multiplicity, and a set of inclusive validation regions targeting different regions of phase space considered in the analysis (i.e. in and out the Z boson mass window, high and low E_T^{miss}, and vetoing events with a trilepton invariant mass within the Z boson mass window). The definitions of the control and validation regions used in the 3ℓ analysis are shown in Table 7. Other background sources such as VVV, tV and Higgs processes contributing to the irreducible background are taken from MC.

In addition to processes listed for the reducible backgrounds in the 2ℓ channels, the reducible backgrounds in the 3ℓ channel also include Z+jets, $t\bar{t}$, WW and in general any physics process leading to less than three prompt and isolated leptons. The reducible backgrounds in the 3ℓ channel are estimated using a data-driven fake factor (FF) method [85]. This method uses two sets of lepton identification criteria; the tight, or "ID" criteria corresponding to the signal lepton selection used in the analysis and the orthogonal loose, or "anti-ID" criteria which is designed to be enriched in FNP leptons. In particular for the anti-ID leptons the isolation and identification requirements applied to signal leptons are reversed. The Z+jets, and $Z+\gamma$ background events in the signal, control and validation regions are estimated using p_T-dependent fake factors, defined as the ratio of the number ID to anti-ID leptons in a FNP-dominated region. These fake factors are then applied to events passing identical selection requirements to the signal, control or validation region in question but where one of the ID leptons is replaced by an anti-ID lepton. The remaining "top-like" reducible background contributions, that include $t\bar{t}$, Wt, and WW, are treated

3ℓ control and validation region definitions						
	$p_T^{\ell_3}$ [GeV]	m_{SFOS} [GeV]	E_T^{miss} [GeV]	m_T^{min} [GeV]	n non$-b-$tagged jets	n $b-$tagged jets
CR3-WZ-inc	> 20	81.2–101.2	> 120	< 110	–	0
CR3-WZ-0j	> 20	81.2–101.2	> 60	< 110	0	0
CR3-WZ-1j	> 20	81.2–101.2	> 120	< 110	> 0	0
VR3-Za	> 30	81.2–101.2	40–60	–	–	–
VR3-Zb	> 30	81.2–101.2	>60	–	–	> 0
VR3-offZa	> 30	$\notin$ [81.2, 101.2]	40–60	–	–	–
VR3-offZb	> 20		> 40	–	–	> 0
VR3-Za-0J	> 20	81.2–101.2	40–60	–	0	0
VR3-Za-1J			40–60	–	> 0	0

Table 7: Control and validation regions used in the 3ℓ channel.

differently: data-to-MC scale factors derived with DF opposite-sign events are applied to simulated SF events.

8 Systematic uncertainties

Several sources of experimental and theoretical systematic uncertainties are considered in the SM background estimates and signal expectations and are included in the profile likelihood fit described in Section 7. The primary sources of systematic uncertainties are related to the jet energy scale (JES) and resolution (JER), the MC modelling, the re-weighting procedure applied to simulation to match the distribution of the number of reconstructed vertices observed in data, the systematic uncertainty considered in the non-prompt background estimation and the theoretical cross section uncertainties. The uncertainty related to the finite statistics of the simulated event samples is taken into account as well. The effects of these uncertainties have been evaluated for all signal samples and background processes. In the 2ℓ+0jets and 3ℓ channels the normalisation of the MC prediction for the dominant background processes is extracted in dedicated control regions. Therefore the systematic uncertainties only affect the extrapolation to the signal regions in these cases.

The JES and JER uncertainties are derived as a function of the p_T and η of the jet, as well as of the pileup conditions and the jet flavour composition of the selected jet sample. They are determined using a combination of simulated samples and data samples, through measurements of the jet response asymmetry in dijet, Z+jets and γ+jets events [72].

The systematic uncertainties related to the modelling of E_T^{miss} in the simulation are estimated by propagating the uncertainties on the energy and momentum scale of each of the physics objects, as well as the uncertainties on the soft term resolution and scale [78].

The remaining detector-related systematic uncertainties, such as those on lepton reconstruction efficiency, energy scale, energy resolution and on the modelling of the trigger [67, 86], are included but have been found to be negligible in all channels.

15

The uncertainties coming from the modelling of diboson events in MC are estimated by varying the renormalisation, factorisation and merging scales used to generate the samples, and the PDFs. In the 2ℓ+0jets channel the impact of these uncertainties on the modelling of Z/γ+jets events is also considered, as well as uncertainties on the modelling of $t\bar{t}$ events due to parton shower simulation (by comparing samples generated with POWHEG + PYTHIA to POWHEG + HERWIG ++ [87]), ISR/FSR modelling (by comparing the predictions of events generated with POWHEG + PYTHIA with two samples where the radiation settings are varied), and the PDF set.

In the 2ℓ+jets channel uncertainties on the data-driven Z+jets estimate are calculated following the methodology used in [81]. An additional uncertainty is based on the difference between the expected background yield from the nominal method and a second method implemented as a cross-check, which extracts the dijet mass shape from data validation regions, normalizes the shape to the sideband regions of the SRs, and extrapolates the background into the W mass peak.

For the matrix method and fake factor estimates of the FNP background, systematic uncertainties are assigned to account for differences between the FNP lepton composition in the SR vs. CR used to derive the fake rates and fake factors. An additional uncertainty is associated to the MC subtraction of prompt leptons from this CR.

The binned SRs in the 2ℓ+0jets and 3ℓ channels are dominated by statistical uncertainties on the background estimates (which range from 10% to 70% in the higher mass regions in the 2ℓ+0jets channel and from 5% to 30% in the 3ℓ channel). The largest systematic uncertaities are the diboson modelling uncertainties, the JES and JER uncertainties and the uncertainties on the $E_{\mathrm{T}}^{\mathrm{miss}}$ modelling. In the 2ℓ+jets channel the dominant uncertainties are the diboson modelling uncertainties ($\sim$ 30%–40%) and the uncertainties associated with the data-driven estimate of the Z+jets background (42%, 71% and 64% in SR2-int,-high and -low (combined) respectively).

9 Results

The HistFitter framework [88], which utilises a profile-likelihood-ratio test [89], is used for the statistical interpretation of the results with the CRs (for the 2ℓ+0jets and 3ℓ channels) and SRs both participating in the fit. The likelihood is built as the product of a Poisson probability density function describing the observed number of events in each CR/SR and Gaussian distributions constraining the nuisance parameters associated with the systematic uncertainties whose widths correspond to the sizes of these uncertainties; Poisson distributions are used instead for MC statistical uncertainties. Correlations of a given nuisance parameter across the different sources of backgrounds and the signal are taken into account when relevant.

In the 2ℓ+0jets and 3ℓ channels, a background-only fit is performed which uses data in the CRs to constrain the nuisance parameters of the likelihood function (these include the normalisation factors for dominant backgrounds and the parameters associated with the systematic uncertainties). In all channels the background estimates are also used to evaluate the agreement between the expected and observed number of events in the validation regions. This agreement is found to be within uncertainties for all the validation regions. For the 2ℓ+0jets channel, the results for the binned regions are shown in Tables 8, 9 and 10 for SF2-SF-a to g, SR2-SF-h to m and SR2-DF-a to d, respectively. The results for the 2ℓ+0jets inclusive signal regions are shown in Table 11, while table 12 summarises the SM background expectation

SR2-	SF-a	SF-b	SF-c	SF-d	SF-e	SF-f	SF-g
Observed	56	28	19	13	10	6	6

Fitted background events

	SF-a	SF-b	SF-c	SF-d	SF-e	SF-f	SF-g
Total SM	47 ± 12	25 ± 5	25 ± 4	14 ± 7	5.2 ± 1.4	1.9 ± 1.2	3.8 ± 1.9
$t\bar{t}$	10 ± 4	7.4 ± 3.5	7.3 ± 3.0	2.7 ± 1.7	–	–	$0.11^{+0.21}_{-0.11}$
Wt	1.0 ± 1.0	1.3 ± 0.7	1.6 ± 0.6	1.1 ± 1.1	–	–	–
VV	21 ± 4	11.3 ± 2.9	12.6 ± 2.4	3.9 ± 2.4	4.4 ± 1.3	1.8 ± 1.2	2.8 ± 1.6
FNP	$2.1^{+2.9}_{-2.1}$	–	–	5 ± 4	–	–	0.9 ± 0.4
Z/γ+jets	13 ± 9	4.7 ± 2.6	3.3 ± 3.2	$1.2^{+1.7}_{-1.2}$	0.7 ± 0.6	$0.02^{+0.21}_{-0.02}$	–
other	0.18 ± 0.08	0.12 ± 0.05	0.11 ± 0.04	0.09 ± 0.05	0.050 ± 0.03	0.03 ± 0.01	0.05 ± 0.02

Expected events before the fit

	SF-a	SF-b	SF-c	SF-d	SF-e	SF-f	SF-g
Total SM	49	26	26	14	5.4	1.9	4.0
$t\bar{t}$	10	8	7.6	2.8	–	–	0.12
Wt	1.0	1.3	1.6	1.1	–	–	–
VV	22	11.7	13.1	4.0	4.6	1.9	2.9
FNP	2.1	–	–	5	–	–	0.9
Z/γ+jets	13	4.7	3.3	1.2	0.7	0.02	–
other	0.18	0.12	0.11	0.09	0.05	0.03	0.05

Table 8: Background-only fit results for SF2-SF-a to g in the 2ℓ+0jets channel. All systematic and statistical uncertainties are included in the fit. The "other" backgrounds include Higgs, VVV and $t\bar{t}V$.

and observed events in the 2ℓ+jets SRs. For the 3ℓ channel, the results are shown in Table 13 for SR3-WZ-0Ja to c and SR3-WZ-1Ja to c (which target gauge-boson-mediated decays) and Table 14 for SR3-slep-a to e. No significant excesses above the SM expectation are observed in any SR.

Figure 2 shows a selection of kinematic distributions for data and the estimated SM backgrounds with their associated statistical and systematic uncertainties for the loosest inclusive SRs in the 2ℓ+0jets channel: SR2-SF-loose and SR2-DF-100. The normalization factors extracted from the corresponding CRs are propagated to the VV and $t\bar{t}$ contributions. Figure 3 shows the $E_{\mathrm{T}}^{\mathrm{miss}}$ distribution in SR2-int, SR2-high and SR2-low of the 2ℓ+jets channel. In the 3ℓ channel, distributions of $E_{\mathrm{T}}^{\mathrm{miss}}$ and the third leading lepton p_{T} are shown for the SR bins targeting $\tilde{\ell}$-mediated decays in Figure 4 while Figure 5 shows distributions of $E_{\mathrm{T}}^{\mathrm{miss}}$ in the bins targeting gauge-boson-mediated decays. Good agreement is observed in all distributions within the uncertainties.

In the absence of SUSY signal, exclusion limits are set on the masses of the charginos and neutralinos for the simplified models considered in the analyses. Figure 6 shows the limits in the 2ℓ+0jets channel on the mass of the $\tilde{\chi}_1^0$ as a function of the $\tilde{\chi}_1^\pm$ mass, for $\tilde{\chi}_1^+\tilde{\chi}_1^-$ pair production with $\tilde{\ell}$-mediated decays, and the limits on the $\tilde{\chi}_1^0$ as a function of $\tilde{\ell}$ mass for direct $\tilde{\ell}\tilde{\ell}$ production. Since the binned signal regions are all mutually orthogonal they are statistically combined. However, for the $\tilde{\ell}\tilde{\ell}$ pair production grid only the same flavour bins are considered as the signal process only contributes SF events. The exclusion limits from the 3ℓ channel for $\tilde{\chi}_1^\pm\tilde{\chi}_2^0$ pair production are shown for $\tilde{\ell}$- and gauge-boson-mediated decays in Figure 7. Finally, the limit on the $\tilde{\chi}_1^\pm$ mass as a function of the degenerate masses of the $\tilde{\chi}_1^\pm$ and the

SR2-	SF-h	SF-i	SF-j	SF-k	SF-l	SF-m
Observed	0	1	3	2	2	7
Fitted background events						
Total SM	3.1 ± 1.0	1.9 ± 0.9	1.6 ± 0.5	1.5 ± 0.6	1.8 ± 0.8	2.6 ± 0.9
$t\bar{t}$	–	–	–	–	–	–
Wt	–	–	–	–	–	–
VV	3.0 ± 1.0	1.5 ± 0.8	1.6 ± 0.5	1.4 ± 0.6	1.7 ± 0.8	2.6 ± 0.9
FNP	–	–	–	–	–	–
Z/γ+jets	$0.02^{+0.11}_{-0.02}$	0.42 ± 0.20	–	$0.02^{+0.20}_{-0.02}$	–	$0.02^{+0.06}_{-0.02}$
other	0.03 ± 0.01	0.03 ± 0.02	–	0.04 ± 0.02	0.02 ± 0.01	0.02 ± 0.02
Expected events before the fit						
Total SM	3.2	2.0	1.7	1.6	1.8	2.7
$t\bar{t}$	–	–	–	–	–	–
Wt	–	–	–	–	–	–
VV	3.1	1.5	1.7	1.5	1.8	2.7
FNP	–	–	–	–	–	–
Z/γ+jets	0.02	0.42	–	0.02	–	0.02
other	0.03	0.03	–	0.04	0.02	0.02

Table 9: Background-only fit results for SR2-SF-h to m in the 2ℓ+0jets channel. All systematic and statistical uncertainties are included in the fit. The "other" backgrounds include Higgs, VVV and $t\bar{t}V$.

$\tilde{\chi}^0_2$ calculated using the 2ℓ+jets channel, is shown in Figure 8. Since the signal regions in this channel are not mutually exclusive, the observed $\mathrm{CL_s}$ value is taken from the signal region with the best expected $\mathrm{CL_s}$ value. For associated $\tilde{\chi}^\pm_1 \tilde{\chi}^0_2$ production, masses up to 1150 GeV are excluded for a 200 GeV $\tilde{\chi}^0_1$ when each gaugino decays via an intermediate $\tilde{\ell}$ to a $\tilde{\chi}^0_1$, and masses up to 380 (580) GeV are excluded for a massless $\tilde{\chi}^0_1$ when gauge-boson-mediated decays are assumed in the case of the 3ℓ (2ℓ+jets) channel. For direct $\tilde{\chi}^+_1 \tilde{\chi}^-_1$ pair production with decays via intermediate $\tilde{\ell}$ to a $\tilde{\chi}^0_1$, masses up to 750 GeV are excluded for a massless $\tilde{\chi}^0_1$ .For $\tilde{\ell}\tilde{\ell}$ pair production where each $\tilde{\ell}$ decays directly to a $\tilde{\chi}^0_1$ and lepton masses up to 500 GeV are excluded for a massless $\tilde{\chi}^0_1$ assuming degenerate left-handed and right-handed $\tilde{\ell}$.

SR2-	DF-a	DF-b	DF-c	DF-d
Observed	67	5	4	2
Fitted background events				
Total SM	57 ± 7	9.6 ± 1.9	$1.5^{+1.7}_{-1.5}$	0.6 ± 0.6
$t\bar{t}$	24 ± 8	–	–	–
Wt	4.5 ± 1.0	–	–	–
VV	26 ± 6	8.8 ± 1.8	$1.5^{+1.7}_{-1.5}$	0.6 ± 0.6
FNP	1.75 ± 0.18	0.57 ± 0.23	–	–
Z/γ+jets	–	–	–	–
other	0.40 ± 0.09	0.17 ± 0.07	0.07 ± 0.07	0.02 ± 0.02
Expected events before the fit				
Total SM	57	9.1	1.5	0.6
$t\bar{t}$	25	–	–	–
Wt	4.5	–	–	–
VV	25	8.4	1.4	0.5
FNP	1.75	0.57	–	–
Z/γ+jets	–	–	–	–
other	0.40	0.17	0.07	0.02

Table 10: Background-only fit results for SR2-DF-a to d in the 2ℓ+0jets channel. All systematic and statistical uncertainties are included in the fit. The "other" backgrounds include Higgs, VVV and $t\bar{t}V$.

SR2-	SF-loose	SF-tight	DF-100	DF-150	DF-200	DF-300
Observed	153	9	78	11	6	2
Fitted background events						
Total SM	133 ± 22	9.8 ± 2.9	68 ± 7	11.5 ± 3.1	2.1 ± 1.9	0.6 ± 0.6
$t\bar{t}$	27 ± 11	–	24 ± 8	–	–	–
Wt	5.0 ± 2.2	–	4.5 ± 1.0	–	–	–
VV	70 ± 11	9.6 ± 3.0	37 ± 8	10.8 ± 3.0	2.0 ± 1.9	0.6 ± 0.6
FNP	6 ± 4	0.0 ± 0.0	2.17 ± 0.29	0.42 ± 0.23	–	–
Z/γ+jets	23 ± 14	$0.09^{+0.34}_{-0.09}$	–	–	–	–
others	0.79 ± 0.23	0.09 ± 0.01	0.67 ± 0.16	0.26 ± 0.08	0.09 ± 0.07	0.02 ± 0.02
Expected events before the fit						
Exp. SM	136	10.2	68	11.0	2.0	0.6
$t\bar{t}$	28	–	25	–	–	–
Wt	5	–	4.5	–	–	–
VV	73	10.0	35	10.3	1.9	0.5
FNP	6.0	0.0	2.17	0.42	–	–
Z/γ+jets	23	0.09	–	–	–	–
others	0.79	0.09	0.67	0.26	0.09	0.02

Table 11: Background-only fit results for the inclusive signal regions in the 2ℓ+0jets channel. All systematic and statistical uncertainties are included in the fit. The "other" backgrounds include Higgs, VVV and $t\bar{t}V$.

SR2-	int	high	low (combined)
Observed	2	0	11
Expected events			
Total SM	4.1 ± 2.6	1.6 ± 1.6	4.2 ± 3.8
VV	4.0 ± 1.8	1.6 ± 1.1	1.7 ± 1.0
$t\bar{t}$	0.15 ± 0.11	0.04 ± 0.03	0.8 ± 0.4
FNP	$0.0^{+0.2}_{-0.0}$	$0.0^{+0.1}_{-0.0}$	$0.7^{+1.8}_{-0.7}$
Z+jets	$0.0^{+1.8}_{-0.0}$	$0.0^{+1.2}_{-0.0}$	$1.0^{+2.7}_{-1.0}$

Table 12: SM background results in the 2ℓ+jets SRs. All systematic and statistical uncertainties are included.

SR3-	WZ-0Ja	WZ-0Jb	WZ-0Jc	WZ-1Ja	WZ-1Jb	WZ-1Jc
Observed	21	1	2	1	3	4

Fitted background events

	WZ-0Ja	WZ-0Jb	WZ-0Jc	WZ-1Ja	WZ-1Jb	WZ-1Jc
Total SM	21.74 ± 2.85	2.68 ± 0.46	1.56 ± 0.33	2.21 ± 0.53	1.82 ± 0.26	1.26 ± 0.34
WZ	19.48 ± 2.90	2.46 ± 0.46	1.33 ± 0.31	1.79 ± 0.48	1.49 ± 0.22	0.92 ± 0.28
ZZ	0.81 ± 0.23	0.06 ± 0.03	0.05 ± 0.01	0.05 ± 0.02	0.02 ± 0.01	0.02 ± 0.00
VVV	0.31 ± 0.07	0.13 ± 0.04	0.13 ± 0.03	0.11 ± 0.02	0.12 ± 0.03	0.23 ± 0.05
$t\bar{t}$V	0.04 ± 0.02	0.01 ± 0.01	0.01 ± 0.01	0.14 ± 0.04	0.12 ± 0.02	0.08 ± 0.02
Higgs	–	–	–	0.01 ± 0.00	–	–
FNP	1.10 ± 0.54	0.02 ± 0.01	0.04 ± 0.02	0.11 ± 0.06	0.07 ± 0.04	0.01 ± 0.00

Expected events before the fit

	WZ-0Ja	WZ-0Jb	WZ-0Jc	WZ-1Ja	WZ-1Jb	WZ-1Jc
Total SM	20.37	2.51	1.47	2.32	1.91	1.32
WZ	18.12	2.29	1.23	1.90	1.58	0.97
ZZ	0.81	0.06	0.05	0.05	0.02	0.02
VVV	0.31	0.13	0.13	0.11	0.12	0.23
$t\bar{t}$V	0.04	0.01	0.01	0.14	0.12	0.08
Higgs	–	–	–	0.01	–	–
FNP	1.09	0.02	0.04	0.11	0.07	0.01

Table 13: Background only fits for SR3-WZ-0Ja to c and SR3-WZ-1Ja to c in the 3ℓ channel. All systematic and statistical uncertainties are included in the fit.

SR3-	slep-a	slep-b	slep-c	slep-d	slep-e
Observed	4	3	9	0	0

Fitted background events					
Total SM	2.23 ± 0.79	2.79 ± 0.43	5.41 ± 0.93	1.42 ± 0.38	1.14 ± 0.23
WZ	1.08 ± 0.38	1.98 ± 0.31	3.85 ± 0.70	0.91 ± 0.26	0.76 ± 0.17
ZZ	0.02 ± 0.01	$0.01^{+0.01}_{-0.01}$	0.13 ± 0.03	0.06 ± 0.02	0.03 ± 0.01
VVV	0.26 ± 0.08	0.34 ± 0.05	0.72 ± 0.12	0.36 ± 0.10	0.25 ± 0.05
$t\bar{t}V$	0.07 ± 0.03	0.09 ± 0.02	0.20 ± 0.04	0.07 ± 0.02	0.02 ± 0.01
Higgs	0.01 ± 0.00	0.01 ± 0.01	0.03 ± 0.02	0.01 ± 0.00	–
FNP	0.80 ± 0.46	0.36 ± 0.18	0.48 ± 0.25	–	0.08 ± 0.04

Expected events before the fit					
Total SM	2.27	2.87	5.55	1.45	1.1
WZ	1.12	2.06	3.99	0.94	0.78
ZZ	0.02	0.01	0.13	0.06	0.03
VVV	0.26	0.34	0.71	0.36	0.25
$t\bar{t}V$	0.07	0.09	0.20	0.07	0.02
Higgs	0.01	0.01	0.03	0.01	–
FNP	0.80	0.36	0.48	–	0.08

Table 14: Background only fits for SR3-slep-a to e in the 3ℓ channel. All systematic and statistical uncertainties are included in the fit.
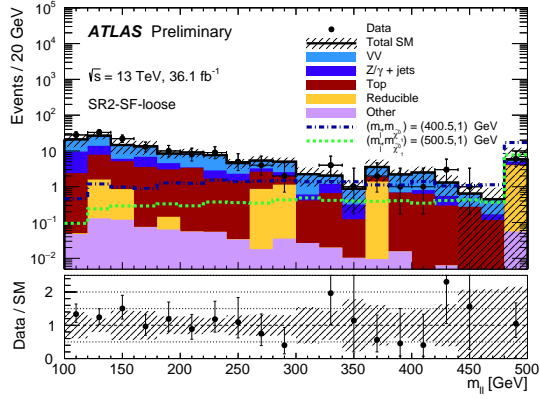
(a) $m_{\ell\ell}$ distribution in SR2-SF-loose
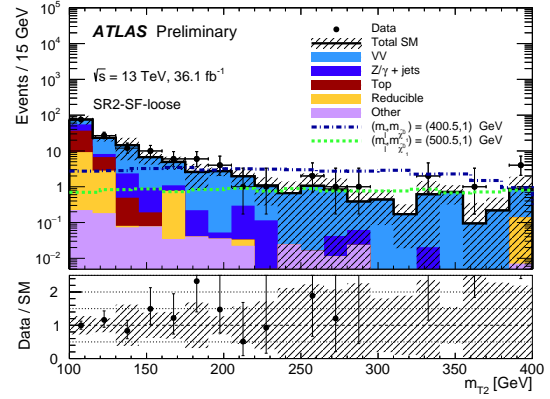
(b) m_{T2} distribution in SR2-SF-loose
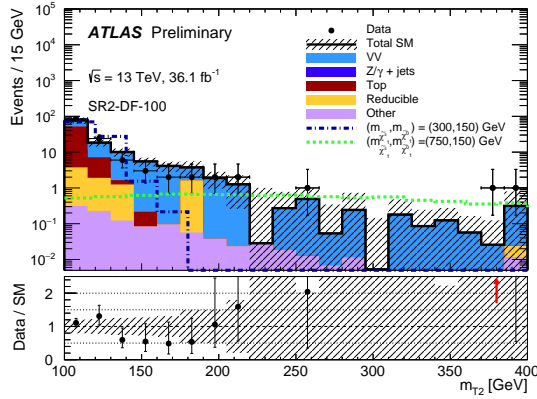
(c) m_{T2} distribution in SR2-DF-100

Figure 2: $m_{\ell\ell}$ (a) and m_{T2} (b) distributions for data and the estimated SM backgrounds in the 2ℓ+0jets channel for SR2-SF-loose and m_{T2} distributions for SR2-DF-100 (c). The normalization factors extracted from the corresponding CRs are used to rescale the $t\bar{t}$ and VV contributions. The "Reducible" category corresponds to the data-driven matrix method estimate. The statistical uncertainties on the background prediction are included in the uncertainty band, as well as the experimental and theoretical uncertainties. The final bins in each histogram also contain the events in the overflow bin.

(a) E_T^{miss} distribution in SR2-int/high

(b) E_T^{miss} distribution in SR2-low
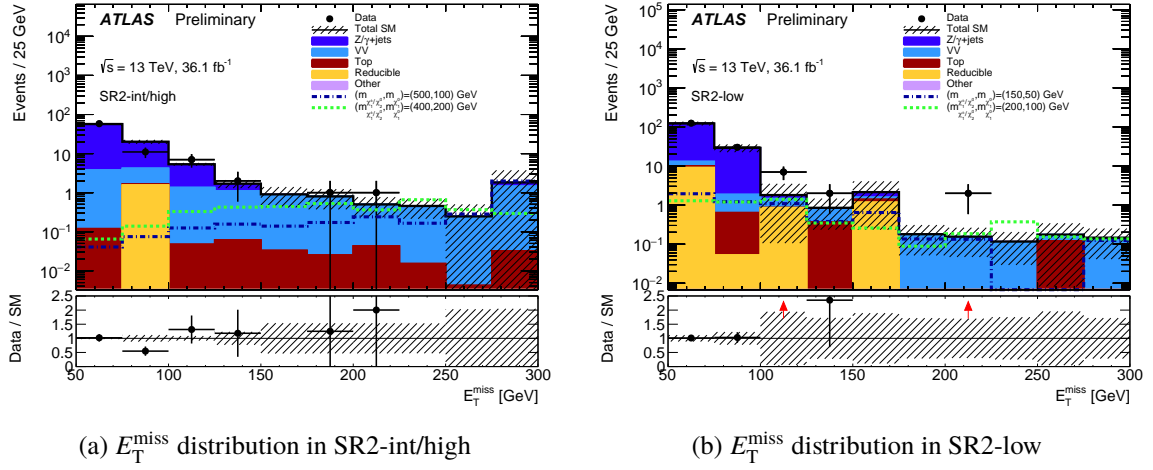
Figure 3: E_T^{miss} distributions of data and the expected SM backgrounds in the 2ℓ+jets channel for SR2-int/high (a) and SR2-low (b), without the final E_T^{miss} requirement applied. The Z/γ+jets contribution is evaluated using the data-driven photon method and the "Reducible" category corresponds to the data-driven matrix method estimate. The statistical uncertainties on the background prediction are included in the uncertainty band, as well as the experimental and theoretical uncertainties.
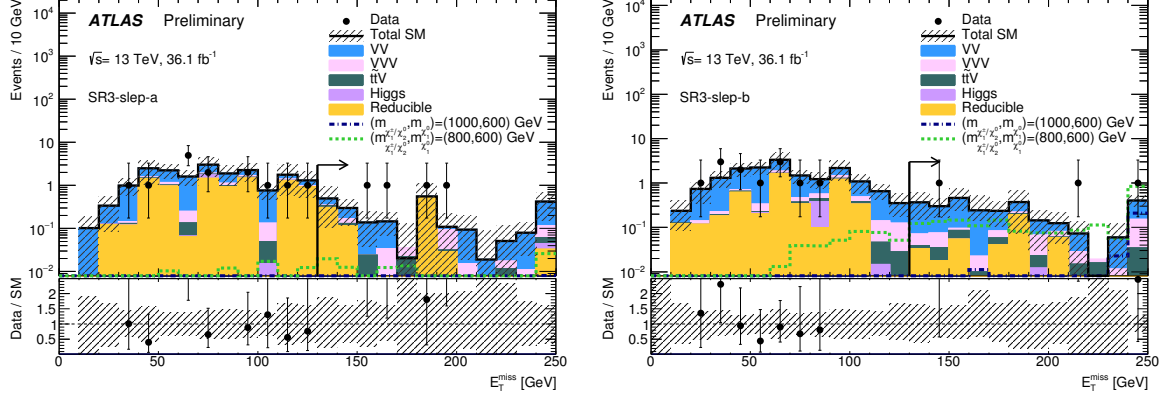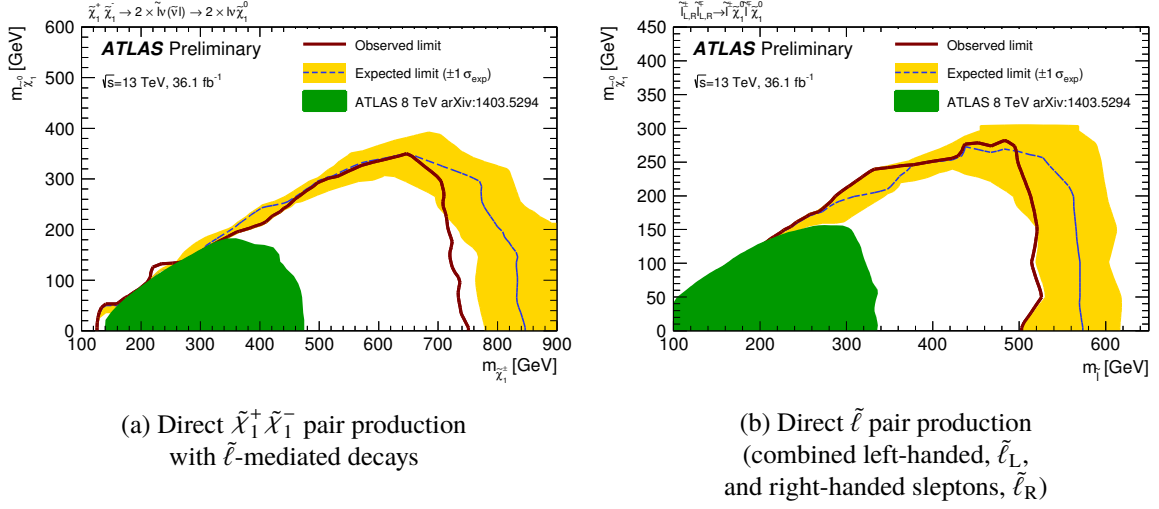
(a) E_T^{miss} distribution in SR3-slep-a

(b) E_T^{miss} distribution in SR3-slep-b
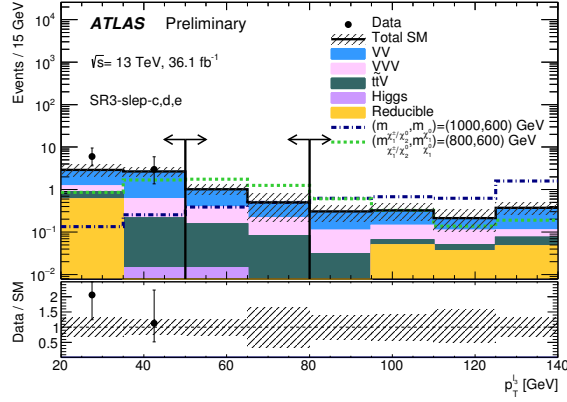
(c) Distribution of third leading lepton p_T in SR3-slep-c to e

Figure 4: E_T^{miss} distributions for data and the estimated SM backgrounds in the 3ℓ channel for SR3-slep-a (a) and SR3-slep-b (b) and distributions of the third leading lepton p_T in SR3-slep-c to e (c) The normalization factors extracted from the corresponding CRs are used to rescale the WZ background. The "Reducible" category corresponds to the data-driven fake factor estimate. The statistical uncertainties on the background prediction are included in the uncertainty band, as well as the experimental and theoretical uncertainties.

(a) E_T^{miss} distribution in SR3-WZ-0Ja to c

(b) E_T^{miss} distribution in SR3-WZ-1Ja

(c) E_T^{miss} distribution SR3-WZ-1Jb

(d) E_T^{miss} distribution SR3-WZ-1Jc
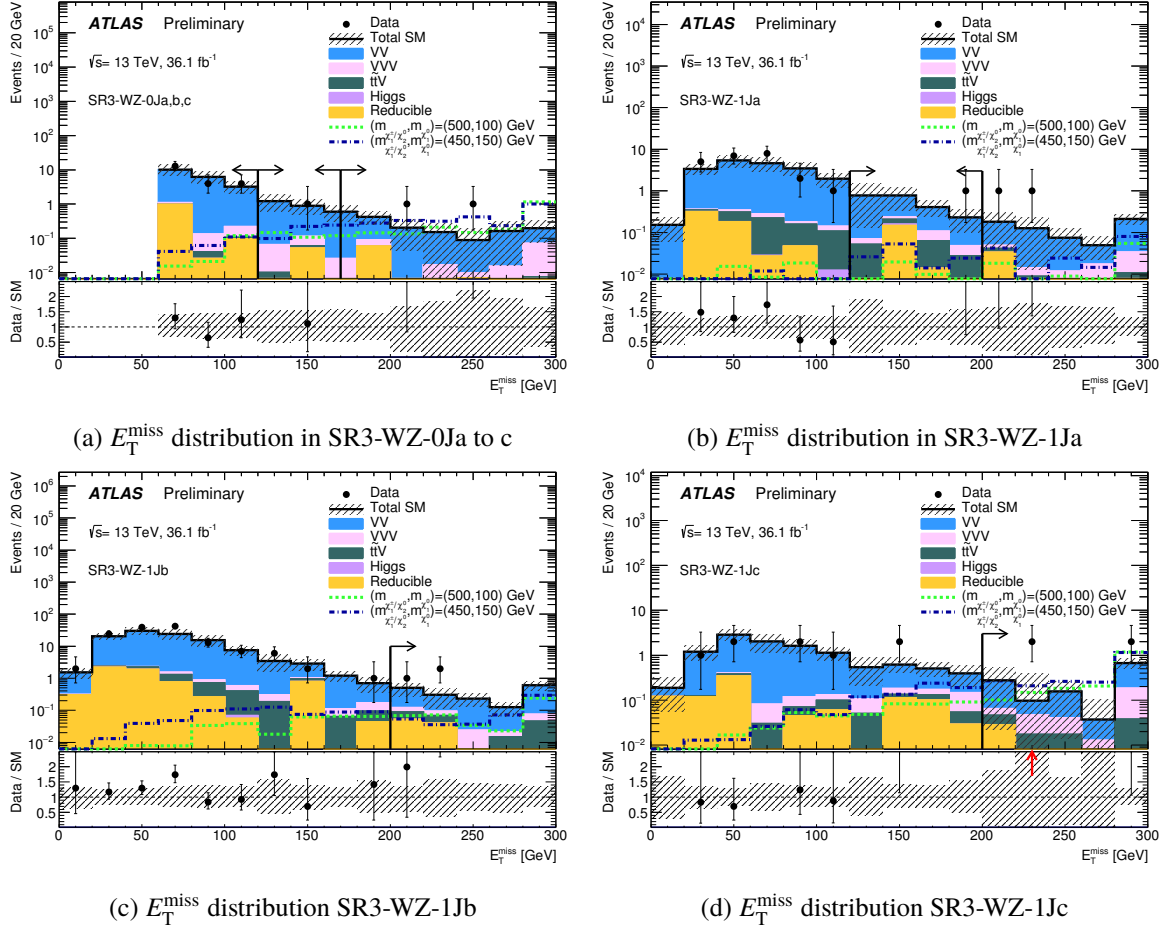
Figure 5: E_T^{miss} distributions for data and the estimated SM backgrounds in the 3ℓ channel for SR3-WZ-0Ja to c (a), SR3-WZ-1Ja (b), SR3-WZ-1Jb (c) and SR3-WZ-1Jc (d). The normalization factors extracted from the corresponding CRs are used to rescale the 0-jet and $\geq$ 1-jet WZ background components. The "Reducible" category corresponds to the data-driven fake factor estimate. The statistical uncertainties on the background prediction are included in the uncertainty band, as well as the experimental and theoretical uncertainties.

(a) Direct $\tilde{\chi}_1^+ \tilde{\chi}_1^-$ pair production
with $\tilde{\ell}$-mediated decays

(b) Direct $\tilde{\ell}$ pair production
(combined left-handed, $\tilde{\ell}_L$,
and right-handed sleptons, $\tilde{\ell}_R$)
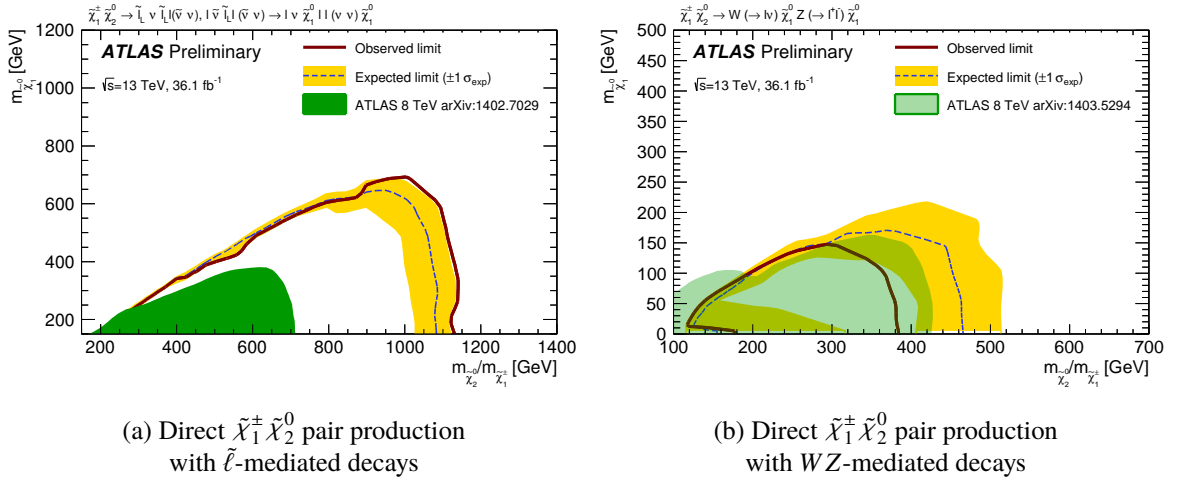
Figure 6: Observed and expected exclusion limits on the $\tilde{\chi}_1^\pm$, $\tilde{\ell}$ and $\tilde{\chi}_1^0$ masses in the context of SUSY scenarios with simplified mass spectra for direct $\tilde{\chi}_1^+ \tilde{\chi}_1^-$ pair production (a) and direct $\tilde{\ell}$ pair production (b) using the 2ℓ+0jets signal regions. For $\tilde{\chi}_1^+ \tilde{\chi}_1^-$ pair production all SF and DF bins are used whereas for $\tilde{\ell}$ pair production only the SF channels are considered. The contours of the band around the expected limit are the $\pm 1\sigma$ results, including all uncertainties except theoretical uncertainties on the signal cross-section. All limits are computed at 95% CL. The observed limits obtained from ATLAS in Run I are also shown [22]. *These plots have been updated since the versions released for the LHCP conference.*

(a) Direct $\tilde{\chi}_1^\pm \tilde{\chi}_2^0$ pair production
with $\tilde{\ell}$-mediated decays

(b) Direct $\tilde{\chi}_1^\pm \tilde{\chi}_2^0$ pair production
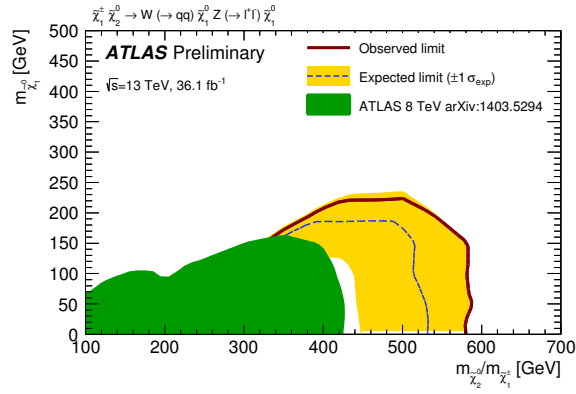with WZ-mediated decays

Figure 7: Observed and expected exclusion limits on the $\tilde{\chi}_1^0$ and the degenerate $\tilde{\chi}_2^0$ and $\tilde{\chi}_1^\pm$ masses in the context of SUSY scenarios with simplified mass spectra for direct $\tilde{\chi}_1^\pm \tilde{\chi}_2^0$ pair production with $\tilde{\ell}$-mediated decays using a statistical combination of SR3-slep-a to c (a) and WZ-mediated decays using a statistical combination of SR3-WZ-0Ja to c and SR3-WZ-1Ja to c. The contours of the band around the expected limit are the $\pm 1\sigma$ results, including all uncertainties except theoretical uncertainties on the signal cross-section. All limits are computed at 95% CL. The observed limits obtained from ATLAS in Run I are also shown [22, 23].

27

Figure 8: Observed and expected exclusion limits on the $\tilde{\chi}_1^0$ and the degenerate $\tilde{\chi}_2^0$ and $\tilde{\chi}_1^\pm$ masses in the context of SUSY scenarios with simplified mass spectra for direct $\tilde{\chi}_1^\pm \tilde{\chi}_2^0$ pair production with decays via gauge bosons to final states involving two leptons and at least two jets. Since the 2ℓ+jets SRs are not orthogonal the observed result for each grid point is taken from the SR with the best expected sensitivity. The contours of the band around the expected limit are the $\pm 1\sigma$ results, including all uncertainties except theoretical uncertainties on the signal cross-section. All limits are computed at 95% CL. The observed limits obtained from ATLAS in Run I are also shown [22].

10 Conclusion

Searches for the electroweak production of neutralinos, charginos and sleptons decaying into final states with exactly two or three electrons or muons and missing transverse momentum are performed using 36.1 fb^{-1} of $\sqrt{s}$=13 TeV proton-proton collisions recorded by the ATLAS detector at the Large Hadron Collider. Three different search channels are considered. The 2ℓ+0jets channel targets direct $\tilde{\chi}_1^+\tilde{\chi}_1^-$ pair production where each $\tilde{\chi}_1^\pm$ decays via an intermediate $\tilde{\ell}$ to a $\tilde{\chi}_1^0$, and direct $\tilde{\ell}\tilde{\ell}$ pair production. The 2ℓ+jets channel targets associated $\tilde{\chi}_1^\pm\tilde{\chi}_2^0$ production where each sparticle decays via a SM gauge boson giving a final state with two leptons consistent with a Z boson and two jets consistent with a W boson. Finally the 3ℓ channel targets associated $\tilde{\chi}_1^\pm\tilde{\chi}_2^0$ production with decays via either intermediate $\tilde{\ell}$ or gauge bosons.

No significant excess above the SM expectation is observed in any of the signal regions considered across the three channels, and the results are used to calculate exclusion limits in several simplified model scenarios. For associated $\tilde{\chi}_1^\pm\tilde{\chi}_2^0$ production with $\tilde{\ell}$-mediated decays, masses up to 1150 GeV are excluded for a 200 GeV $\tilde{\chi}_1^0$. Both the 2ℓ+jets and 3ℓ channels place exclusion limits on associated $\tilde{\chi}_1^\pm\tilde{\chi}_2^0$ production with gauge-boson-mediated decays. For a massless $\tilde{\chi}_1^0$, $\tilde{\chi}_1^\pm/\tilde{\chi}_2^0$ masses up to approximately 380 GeV are excluded in the 3ℓ channel and masses up to 580 GeV are excluded in the 2ℓ+jets channel. In the 2ℓ+0jets channel, for direct $\tilde{\chi}_1^+\tilde{\chi}_1^-$ pair production with decays via intermediate $\tilde{\ell}$ to a $\tilde{\chi}_1^0$, masses up to 750 GeV are excluded for a massless $\tilde{\chi}_1^0$ and for $\tilde{\ell}\tilde{\ell}$ pair production masses up to 500 GeV are excluded for a massless $\tilde{\chi}_1^0$ assuming degenerate left-handed and right-handed sleptons.

References

[1] Yu. A. Golfand and E. P. Likhtman, *Extension of the Algebra of Poincare Group Generators and Violation of p Invariance*, JETP Lett. **13** (1971) 323.

[2] D. V. Volkov and V. P. Akulov, *Is the Neutrino a Goldstone Particle?*, Phys. Lett. B **46** (1973) 109.

[3] J. Wess and B. Zumino, *Supergauge Transformations in Four-Dimensions*, Nucl. Phys. B **70** (1974) 39.

[4] J. Wess and B. Zumino, *Supergauge Invariant Extension of Quantum Electrodynamics*, Nucl. Phys. B **78** (1974) 1.

[5] S. Ferrara and B. Zumino, *Supergauge Invariant Yang-Mills Theories*, Nucl. Phys. B **79** (1974) 413.

[6] A. Salam and J. A. Strathdee, *Supersymmetry and Nonabelian Gauges*, Phys. Lett. B **51** (1974) 353.

[7] S. P. Martin, *A Supersymmetry primer*, (1997), [Adv. Ser. Direct. High Energy Phys.18,1(1998)], arXiv: hep-ph/9709356.

[8] P. Fayet, *Supersymmetry and Weak, Electromagnetic and Strong Interactions*, Phys. Lett. B **64** (1976) 159.

[9] P. Fayet, *Spontaneously Broken Supersymmetric Theories of Weak, Electromagnetic and Strong Interactions*, Phys. Lett. B **69** (1977) 489.

[10] N. Sakai, *Naturalness in Supersymmetric GUTS*, Z. Phys. C **11** (1981) 153.

[11] S. Dimopoulos, S. Raby and F. Wilczek, *Supersymmetry and the Scale of Unification*, Phys. Rev. D **24** (1981) 1681.

[12] L. E. Ibanez and G. G. Ross, *Low-Energy Predictions in Supersymmetric Grand Unified Theories*, Phys. Lett. B **105** (1981) 439.

[13] S. Dimopoulos and H. Georgi, *Softly Broken Supersymmetry and SU(5)*, Nucl. Phys. B **193** (1981) 150.

[14] G. R. Farrar and P. Fayet, *Phenomenology of the Production, Decay, and Detection of New Hadronic States Associated with Supersymmetry*, Phys. Lett. B **76** (1978) 575.

[15] H. Goldberg, *Constraint on the Photino Mass from Cosmology*, Phys. Rev. Lett. **50** (1983) 1419, [Erratum: Phys. Rev. Lett. 103 (2009) 099905].

[16] J. R. Ellis, J. S. Hagelin, D. V. Nanopoulos, K. A. Olive and M. Srednicki, *Supersymmetric Relics from the Big Bang*, Nucl. Phys. B **238** (1984) 453.

[17] L. Evans and P. Bryant, *LHC Machine*, JINST **3** (2008) S08001.

[18] ATLAS Collaboration, *The ATLAS Experiment at the CERN Large Hadron Collider*, JINST **3** (2008) S08003.

[19] CMS Collaboration, *The CMS experiment at the CERN LHC*, JINST **3** (2008) S08004.

[20] ATLAS Collaboration, *Search for squarks and gluinos in final states with jets and missing transverse momentum at $\sqrt{s}$ = 13 TeV with the ATLAS detector*, Eur. Phys. J. C **76** (2016) 392, arXiv: 1605.03814 [hep-ex].

[21] CMS Collaboration, *Inclusive search for supersymmetry using razor variables in pp collisions at $\sqrt{s}$ = 13 TeV*, Phys. Rev. D **95** (2017) 012003, arXiv: 1609.07658 [hep-ex].

[22] ATLAS Collaboration, *Search for direct production of charginos, neutralinos and sleptons in final states with two leptons and missing transverse momentum in pp collisions at $\sqrt{s}$ = 8 TeV with the ATLAS detector*, JHEP **05** (2014) 071, arXiv: 1403.5294 [hep-ex].

[23] ATLAS Collaboration, *Search for direct production of charginos and neutralinos in events with three leptons and missing transverse momentum in $\sqrt{s}$ = 8 TeV pp collisions with the ATLAS detector*, JHEP **04** (2014) 169, arXiv: 1402.7029 [hep-ex].

[24] ATLAS collaboration, *Search for the electroweak production of supersymmetric particles in $\sqrt{s}$=8 TeV pp collisions with the ATLAS detector*, Phys. Rev. D **93** (2016) 052002, arXiv: 1509.07152 [hep-ex].

[25] CMS Collaboration, *Searches for electroweak neutralino and chargino production in channels with Higgs, Z, and W bosons in pp collisions at 8 TeV*, Phys. Rev. D **90** (2014) 092007, arXiv: 1409.3168 [hep-ex].

[26] CMS collaboration, *Searches for electroweak production of charginos, neutralinos, and sleptons decaying to leptons and W, Z, and Higgs bosons in pp collisions at 8 TeV*, Eur. Phys. J. C **74** (2014) 3036, arXiv: 1405.7570 [hep-ex].

[27] J. Alwall, P. Schuster and N. Toro, *Simplified Models for a First Characterization of New Physics at the LHC*, Phys. Rev. D **79** (2009) 075020, arXiv: 0810.3921 [hep-ph].

[28] ATLAS Collaboration, *ATLAS Insertable B-Layer Technical Design Report*, CERN-LHCC-2010-013. ATLAS-TDR-19, 2010, URL: http://cds.cern.ch/record/1291633.

[29] ATLAS Collaboration, *Performance of the ATLAS Trigger System in 2015*, (2016), arXiv: 1611.09661 [hep-ex].

[30] ATLAS Collaboration, *Improved luminosity determination in pp collisions at $\sqrt{s}$ = 7 TeV using the ATLAS detector at the LHC*, Eur. Phys. J. C **73** (2013) 2518, arXiv: 1302.4393 [hep-ex].

[31] ATLAS Collaboration, *Luminosity determination in pp collisions at $\sqrt{s}$ = 8 TeV using the ATLAS detector at the LHC*, Eur. Phys. J. C **76** (2016) 653, arXiv: 1608.03953 [hep-ex].

[32] ATLAS Collaboration, *The ATLAS Simulation Infrastructure*, Eur. Phys. J. C **70** (2010) 823, arXiv: 1005.4568 [hep-ex].

[33] S. Agostinelli et al., *GEANT4: A Simulation toolkit*, Nucl. Instrum. Meth. A **506** (2003) 250.

[34] ATLAS Collaboration, *The simulation principle and performance of the ATLAS fast calorimeter simulation FastCaloSim*, ATL-PHYS-PUB-2010-013, 2010, URL: https://cds.cern.ch/record/1300517.

[35] T. Gleisberg, S. Höche, F. Krauss, M. Schönherr, S. Schumann et al., *Event generation with SHERPA 1.1*, JHEP **02** (2009) 007, arXiv: 0811.4622 [hep-ph].

[36] ATLAS Collaboration, *Multi-boson simulation for 13 TeV ATLAS analyses*, ATL-PHYS-PUB-2016-002, 2016, URL: https://cds.cern.ch/record/2119986.

[37] T. Gleisberg and S. Höche, *Comix, a new matrix element generator*, JHEP **12** (2008) 039, arXiv: 0808.3674 [hep-ph].

[38] F. Cascioli, P. Maierhofer and S. Pozzorini, *Scattering Amplitudes with Open Loops*, Phys. Rev. Lett. **108** (2012) 111601, arXiv: 1111.5206 [hep-ph].

[39] S. Schumann and F. Krauss, *A Parton shower algorithm based on Catani-Seymour dipole factorisation*, JHEP **03** (2008) 038, arXiv: 0709.1027 [hep-ph].

[40] S. Höche, F. Krauss, M. Schönherr and F. Siegert, *QCD matrix elements + parton showers: The NLO case*, JHEP **04** (2013) 027, arXiv: 1207.5030 [hep-ph].

[41] R. D. Ball et al., *Parton distributions for the LHC Run II*, JHEP **04** (2015) 040, arXiv: 1410.8849 [hep-ph].

[42] H.-L. Lai et al., *New parton distributions for collider physics*, Phys. Rev. D **82** (2010) 074024, arXiv: 1007.2241 [hep-ph].

[43] ATLAS Collaboration, *Monte Carlo Generators for the Production of a W or Z/γ* Boson in Association with Jets at ATLAS in Run 2*, ATL-PHYS-PUB-2016-003, 2016, URL: https://cds.cern.ch/record/2120133.

[44] F. P. R. Gavin Y. Li and S. Quackenbush, *FEWZ 2.0: A code for hadronic Z production at next-to-next-to-leading order*, Comput. Phys. Commun. **182** (2011) 2388, arXiv: 1011.3540 [hep-ph].

[45] E. Re, *Single-top Wt-channel production matched with parton showers using the POWHEG method*, Eur. Phys. J. C **71** (2011) 1547, arXiv: 1009.2450 [hep-ph].

[46] S. Frixione, P. Nason and G. Ridolfi, *A Positive-weight next-to-leading-order Monte Carlo for heavy flavour hadroproduction*, JHEP **09** (2007) 126, arXiv: 0707.3088 [hep-ph].

[47] ATLAS Collaboration, *Simulation of top-quark production for the ATLAS experiment at $\sqrt{s}$ = 13 TeV*, ATL-PHYS-PUB-2016-004, 2016, URL: https://cds.cern.ch/record/2120417.

[48] M. Czakon and A. Mitov, *Top++: A Program for the Calculation of the Top-Pair Cross-Section at Hadron Colliders*, Comput. Phys. Commun. **185** (2014) 2930, arXiv: 1112.5675 [hep-ph].

[49] N. Kidonakis, *Two-loop soft anomalous dimensions for single top quark associated production with a W- or H-*, Phys. Rev. **D82** (2010) 054018, arXiv: `1005.4451 [hep-ph]`.

[50] J. Alwall, R. Frederix, S. Frixione, V. Hirschi, F. Maltoni et al., *The automated computation of tree-level and next-to-leading order differential cross sections, and their matching to parton shower simulations*, JHEP **07** (2014) 079, arXiv: `1405.0301 [hep-ph]`.

[51] T. Sjöstrand, S. Mrenna and P. Z. Skands, *A Brief Introduction to PYTHIA 8.1*, Comput. Phys. Commun. **178** (2008) 852, arXiv: `0710.3820 [hep-ph]`.

[52] ATLAS Collaboration, *Modelling of the $t\bar{t}H$ and $t\bar{t}V$ ($V = W, Z$) processes for $\sqrt{s} = 13$ TeV ATLAS analyses*, ATL-PHYS-PUB-2016-005, 2016, URL: `https://cds.cern.ch/record/2120826`.

[53] ATLAS Collaboration, *ATLAS Pythia 8 tunes to 7 TeV data*, ATL-PHYS-PUB-2014-021, 2014, URL: `https://cds.cern.ch/record/1966419`.

[54] R. D. Ball et al., *Parton distributions with LHC data*, Nucl. Phys. B **867** (2013) 244, arXiv: `1207.1303 [hep-ph]`.

[55] S. Alioli, P. Nason, C. Oleari and E. Re, *A general framework for implementing NLO calculations in shower Monte Carlo programs: the POWHEG BOX*, JHEP **06** (2010) 043, arXiv: `1002.2581 [hep-ph]`.

[56] L. Lönnblad and S. Prestel, *Matching Tree-Level Matrix Elements with Interleaved Showers*, JHEP **03** (2012) 019, arXiv: `1109.4829 [hep-ph]`.

[57] W. Beenakker, R. Hopker, M. Spira and P. Zerwas, *Squark and gluino production at hadron colliders*, Nucl. Phys. B **492** (1997) 51, arXiv: `hep-ph/9610490 [hep-ph]`.

[58] A. Kulesza and L. Motyka, *Threshold resummation for squark-antisquark and gluino-pair production at the LHC*, Phys. Rev. Lett. **102** (2009) 111802, arXiv: `0807.2405 [hep-ph]`.

[59] A. Kulesza and L. Motyka, *Soft gluon resummation for the production of gluino-gluino and squark-antisquark pairs at the LHC*, Phys. Rev. D **80** (2009) 095004, arXiv: `0905.4749 [hep-ph]`.

[60] W. Beenakker, S. Brensing, M. Kramer, A. Kulesza, E. Laenen et al., *Soft-gluon resummation for squark and gluino hadroproduction*, JHEP **0912** (2009) 041, arXiv: `0909.4418 [hep-ph]`.

[61] W. Beenakker, S. Brensing, M. Kramer, A. Kulesza, E. Laenen et al., *Squark and gluino hadroproduction*, Int. J. Mod. Phys. A **26** (2011) 2637, arXiv: `1105.1110 [hep-ph]`.

[62] C. Borschensky et al., *Squark and gluino production cross sections in pp collisions at $\sqrt{s} = 13, 14, 33$ and 100 TeV*, Eur. Phys. J. C **74** (2014) 3174, arXiv: `1407.5066 [hep-ph]`.

[63] D. J. Lange, *The EvtGen particle decay simulation package*, Nucl. Instrum. Meth. A **462** (2001) 152.

[64] ATLAS Collaboration, *Summary of ATLAS Pythia 8 tunes*, ATLAS-PHYS-PUB-2012-003, 2012, URL: `http://cdsweb.cern.ch/record/1474107`.

[65] A. D. Martin, W. J. Stirling, R. S. Thorne and G. Watt, *Parton distributions for the LHC*, Eur. Phys. J. C **63** (2009) 189, arXiv: `0901.0002 [hep-ph]`.

[66] ATLAS Collaboration, *Vertex Reconstruction Performance of the ATLAS Detector at $\sqrt{s} = 13$ TeV*, ATL-PHYS-PUB-2015-026, 2015, URL: `https://cds.cern.ch/record/2037717`.

[67] ATLAS Collaboration, *Electron identification measurements in ATLAS using $\sqrt{s} = 13$ TeV data with 50 ns bunch spacing*, ATL-PHYS-PUB-2015-041, 2015, URL: `https://cds.cern.ch/record/2048202`.

[68] ATLAS Collaboration, *Electron efficiency measurements with the ATLAS detector using 2012 LHC proton–proton collision data*, (2016), arXiv: 1612.01456 [hep-ex].

[69] ATLAS Collaboration, *Muon reconstruction performance of the ATLAS detector in proton–proton collision data at $\sqrt{s}$ = 13 TeV*, Eur. Phys. J. C **76** (2016) 292, arXiv: 1603.05598 [hep-ex].

[70] M. Cacciari, G. P. Salam and G. Soyez, *The anti-kt jet clustering algorithm*, JHEP **04** (2008) 063, arXiv: 0802.1189 [hep-ph].

[71] W. Lampl et al., *Calorimeter Clustering Algorithms: Description and Performance*, ATL-LARG-PUB-2008-002, 2008, URL: https://cds.cern.ch/record/1099735.

[72] ATLAS Collaboration, *Jet Calibration and Systematic Uncertainties for Jets Reconstructed in the ATLAS Detector at $\sqrt{s}$ = 13 TeV*, ATL-PHYS-PUB-2015-015, 2015, URL: https://cds.cern.ch/record/2037613.

[73] ATLAS Collaboration, *Tagging and suppression of pileup jets with the ATLAS detector*, ATLAS-CONF-2014-018, 2014, URL: https://cds.cern.ch/record/1700870.

[74] ATLAS Collaboration, *Optimisation of the ATLAS b-tagging performance for the 2016 LHC Run*, ATL-PHYS-PUB-2016-012, 2016, URL: https://cds.cern.ch/record/2160731.

[75] ATLAS Collaboration, *Performance of b-Jet Identification in the ATLAS Experiment*, JINST **11** (2016) P04008, arXiv: 1512.01094 [hep-ex].

[76] ATLAS Collaboration, *Measurement of the photon identification efficiencies with the ATLAS detector using LHC Run-1 data*, Eur. Phys. J. C **76** (2016) 666, arXiv: 1606.01813 [hep-ex].

[77] ATLAS Collaboration, *Performance of missing transverse momentum reconstruction with the ATLAS detector in the first proton–proton collisions at $\sqrt{s}$ = 13 TeV*, ATL-PHYS-PUB-2015-027, 2015, URL: https://cds.cern.ch/record/2037904.

[78] ATLAS Collaboration, *Expected performance of missing transverse momentum reconstruction for the ATLAS detector at $\sqrt{s}$ = 13 TeV*, ATL-PHYS-PUB-2015-023, 2015, URL: https://cds.cern.ch/record/2037700.

[79] C. G. Lester and D. J. Summers, *Measuring masses of semiinvisibly decaying particles pair produced at hadron colliders*, Phys. Lett. B **463** (1999) 99, arXiv: hep-ph/9906349.

[80] A. Barr, C. Lester and P. Stephens, *m(T2): The Truth behind the glamour*, J. Phys. G **29** (2003) 2343, arXiv: hep-ph/0304226.

[81] ATLAS Collaboration, *Search for new phenomena in events containing a same-flavour opposite-sign dilepton pair, jets, and large missing transverse momentum in $\sqrt{s}$ = 13 TeV pp collisions with the ATLAS detector*, Eur. Phys. J. C **77** (2017) 144, arXiv: 1611.05791 [hep-ex].

[82] CMS Collaboration, *Search for physics beyond the standard model in events with a Z boson, jets, and missing transverse energy in pp collisions at $\sqrt{s}$ = 7 TeV*, Phys. Lett. B **716** (2012) 260, arXiv: 1204.3774 [hep-ex].

[83] CMS Collaboration, *Search for physics beyond the standard model in events with two leptons, jets, and missing transverse momentum in pp collisions at $\sqrt{s}$ = 8 TeV*, JHEP **04** (2015) 124, arXiv: 1502.06031 [hep-ex].

[84] ATLAS Collaboration, *Measurement of the top quark-pair production cross section with ATLAS in pp collisions at $\sqrt{s}$ = 7 TeV*, Eur. Phys. J. C **71** (2011) 1577, arXiv: 1012.1792 [hep-ex].

[85] ATLAS Collaboration, *Measurement of the $W^{\pm}Z$ boson pair-production cross section in pp collisions at $\sqrt{s} = 13$ TeV with the ATLAS Detector*, Phys. Lett. B **762** (2016) 1, arXiv: `1606.04017` `[hep-ex]`.

[86] ATLAS Collaboration, *Muon reconstruction performance in early $\sqrt{s} = 13$ TeV data*, ATL-PHYS-PUB-2015-037, 2015, URL: `https://cds.cern.ch/record/2047831`.

[87] M. Bahr et al., *Herwig++ Physics and Manual*, Eur. Phys. J. C **58** (2008) 639, arXiv: `0803.0883` `[hep-ph]`.

[88] M. Baak et al., *HistFitter software framework for statistical data analysis*, Eur. Phys. J. C **75** (2015) 153, arXiv: `1410.1280 [hep-ex]`.

[89] G. Cowan, K. Cranmer, E. Gross and O. Vitells, *Asymptotic formulae for likelihood-based tests of new physics*, Eur. Phys. J. C **71** (2011) 1554, [Erratum: Eur. Phys. J. **C**73 (2013) 2501], arXiv: `1007.1727 [physics.data-an]`.